On the transient behavior of frictional melt during seismic slip

S. Nielsen,[1] P. Mosca,[2] G.Giberti,[3] G. Di Toro[1,4] T. Hirose[5] T. Shimamoto[6]

S. Nielsen, Istituto Nazionale di Geofisica e Vulcanologia, Dpt. di Sismologia e Tettonofisica, Via di Vigna Murata, 605, 00143 Roma, Italy. (stefan.nielsen@ingv.it)

P. Mosca, Universit di Napoli, Federico II, Dpt. di Scienze Fisiche, Complesso Universitario di Monte Sant'Angelo, via Cintia, I-80126, Napoli, Italy. (paolafly@yahoo.com)

G. Giberti, Universit di Napoli, Federico II, Dpt. di Scienze Fisiche, Complesso Universitario di Monte Sant'Angelo, via Cintia, I-80126, Napoli, Italy. (grazia.giberti@na.infn.it)

G. Di Toro, Istituto Nazionale di Geofisica e Vulcanologia, Dpt. di Sismologia e Tettonofisica, Via di Vigna Murata, 605, 00143 Roma, Italy. (giulio.ditoro@ingv.it)

T. Hirose, Kochi Institute for Core Sample Research, Japan Agency Marine Earth Science and Technology, Kochi, Japan. (hirose@jamstec.go.jp)

T. Shimamoto, Hiroshima University, Dpt. of Earth and Planetary Systems Science, Higashi-Hiroshima, Japan. (shima007@hiroshima-u.ac.jp)

Abstract. In a recent work on the problem of sliding surfaces under the presence of frictional melt (applying in particular to earthquake fault dynamics), we derived from first principles an expression for the steady state friction compatible with experimental observations. Building on the expressions of heat and mass balance obtained in the above study for this particular case of Stefan problem (phase transition with a migrating boundary) we propose here an extension providing the full time-dependent solution (including the weakening transient after pervasive melting has started, the effect of even-

[1] Istituto Nazionale di Geofisica e Vulcanologia, Dpt. di Sismologia e Tettonofisica.

[2] Universit di Napoli, Federico II, Dpt. di Scienze Fisiche, Napoli, Italy.

[4] Universit degli studi di Padova, Dpt. di Geoscienze, Padova, Italy.

[5] Kochi Institute for Core Sample Research, Japan Agency Marine Earth Science and Technology, Kochi, Japan.

[6] Hiroshima University, Dpt. of Earth and Planetary Systems Science, Higashi-Hiroshima, Japan.

tual steps in velocity and the final decelerating phase). A system of coupled equations is derived and solved numerically. The resulting transient friction and wear evolution yield a satisfactory fit (1) with experiments performed under variable sliding velocities (0.9-2 m/s) and different normal stresses (0.5-20 MPa) for various rock types and (2) with estimates of slip weakening obtained from observations on ancient seismogenic faults that host pseudotachylite (solidified melt). The model allows to extrapolate the experimentally observed frictional behavior to large normal stresses representative of the seismogenic Earth crust (up to 200 MPa), high slip rates (up to 9 m/s) and cases where melt extrusion is negligible. Though weakening distance and peak stress vary widely, the net breakdown energy appears to be essentially independent of either slip velocity and normal stress. In addition, the response to earthquake-like slip can be simulated, showing a rapid friction recovery when slip rate drops. We discuss the properties of energy dissipation, transient duration, velocity weakening, restrengthening in the decelerating final slip phase and the implications for earthquake source dynamics.

1. Introduction

It is expected, and observed in many experiments, that heating triggers a series of mechanical, chemical and tribological processes altering the frictional properties of a sliding interface (*Rice*, 2006, and references therein). Such processes may lead to a severe weakening and reduction in friction, especially under high slip rates and normal loads [*Di Toro et al.*, 2006b]. During an earthquake, slip at high rates (¿1 m/s) may produce a very intense heating in a very short time, therefore rapidly weakening the fault and allowing it to accumulate large amounts of slip under a relatively low friction once an initial high friction transient is over. Therefore an initially strong fault can become dynamically weak for the duration of the earthquake, reducing significantly the overall amount of heat production. This may explain why the heat flow observed on several active fault sites, is much smaller that what expected if a persistently high friction coefficient was assumed (see heat flow paradox, *Brune et al.*, 1969), although other explanations not connected to heating have been proposed (e.g., normal vibrations of the fault surface, *Brune et al.*, 1993). In addition, we note that low dynamic friction is compatible with seismological inferences of locally high dynamic stress drops (*Spudich*, 1998) and short slip duration (*Heaton*, 1990; *Zheng and Rice*, 1998; *Nielsen and Madariaga*, 2003).

Several dynamic weakening mechanisms have therefore been proposed and investigated to some extent. In several such mechanisms, the weakening is related to some form of thermally activated process and is triggered by frictional heating. Some well-known examples are fluid pressurization (*Bizzarri and Cocco*, 2006), decarbonation (*Han et al.*, 2007), silica gel formation (*Goldsby and Tullis*, 2002; *Di Toro et al.*, 2004), hydrodynamic lubrication (*Brodsky and Kanamori*, 2001); acoustic fluidization (*Melosh*, 1996); flash heating [*Rice*, 2006; *Beeler et al.*, 2008; *Rempel and Weaver*, 2008]. The present study is dedicated essentially to the case of melting, observed both in laboratory experiments (*Spray*, 1987; *Tsutsumi and Shimamoto*, 1997; *Hirose and Shimamoto*, 2005; *Spray*, 2005; *Di Toro et al.*, 2006b; *Del Gaudio et al.*, 2009) and on natural faults (e.g., ancient faults now found at the surface but originally active at depths of several km in the seimogenic Earth crust or upper mantle, see *Sibson*, 1975; *Swanson*, 1992; *Di Toro and Pennacchioni*, 2004; *Spray*, 2005; *Di Toro et al.*, 2006a; *Ueda et al.*, 2008 and, for a review, *Snoke et al.*, 1998).

This paragraph recalls some of the main points about frictional melt experiments that are useful for the goals of this paper. Melt has been generated in many experiments that impose seismic slip conditions on cohesive samples of silicate-built rocks (e.g., gabbro, tonalite, peridotite, monzodiorite, novaculite), offering useful hints about the physics of friction in the presence of melt [*Tsutsumi and Shimamoto*, 1997; *Hirose and Shimamoto*, 2005; *Di Toro et al.*, 2006b; *Nielsen et al.*, 2008; *Del Gaudio et al.*, 2009]. The rock specimens were cut either into solid cylinders with an external radius $12\,\mathrm{mm} < R < 20\,\mathrm{mm}$, or into hollow annular shapes with an inner void of radius $7.5\,\mathrm{mm} < R_i < 13\,\mathrm{mm}$. They were installed in a rotary shear apparatus and forced to slip one against the other (for a description see *Shimamoto and Tsutsumi*, 1994; *Hirose and Shimamoto*, 2005). In most of these experiments, constant or stepwise constant slip rates V were imposed (V up to 2.6 m/s) while constant normal stresses σ_n were applied (σ_n up to 25 MPa) . During the experiment, the resulting shear stress evolution (friction) was measured. The continued melting and extrusion of melt from the sliding interface induces shortening of the sample which is also monitored. After the end of the experiment the samples were recovered to allow investigations of microstructural and geochemical nature.

The heat balance and the temperature of a sliding interface are governed essentially by the competition between heat production processes (work produced by friction or localized shear) and heat depletion processes (diffusion, transport, heat capacity and latent heat absorbed by phase transitions, ...). An efficient temperature rise, eventually leading to melting or other weakening process, will take place when the heat production rate is high relative to the heat depletion rate. In the presence of frictional melt, the heat source is essentially viscous shear, while heat depletion is caused by diffusion, latent heat and removal of melt by extrusion into the wall rocks. The friction results from viscous shear of a thin melt layer, whose thickness, temperature and viscosity are governed by a system of coupled differential equations [*Fialko and Khazan*, 2005; *Nielsen et al.*, 2008]. Throughout this paper, the resistance to sliding motion resulting from the shearing of the melt will be equally referred to either as shear stress or friction.

In the case of melt removal from the frictional interface (for example by melt extrusion from the sample or injected into side cracks on natural faults, the so-called injection veins, *Sibson*, 1975), a steady state can be reached under a constant slip rate, both observed in laboratory experiments (*Hirose and Shimamoto*, 2005) and predicted by theory (*Nielsen et al.*, 2008). In addition, under steady state conditions, the diffusion equation yields a simple thermal profile, allowing to obtain in closed form the solution of shear stress, melt viscosity and melt thickness (*Nielsen et al.*, 2008).

However, if the steady state is not achieved, the migration of the solid/melt boundary (Stefan problem) at a variable rate, turns the thermal diffusion into a highly non-linear problem which possesses no simple analytical solution (*Landau*, 1950). Therefore, in the present study we extend the analysis of frictional melt of *Nielsen et al.* [2008] to the transient regime, by introducing a numerical solution of the thermal diffusion away from the sliding interface, in the presence of a boundary moving at variable rates and under variable conditions of heat inflow.

As described in section 2 and 3, a system of coupled equations governs the mechanical and thermal balance of the system. Once the heat flow (diffusion) and the heat sink (melting latent heat) are quantified, we can investigate the formation and evolution of the melt layer, its thickness, temperature and viscosity. We derive the viscous flow generated by squeeze due to normal loading, and, finally, obtain the dynamic evolution of friction resulting from viscous shear.

In section 4 we compare the model to results from a number of laboratory experiments on silica-built rocks (gabbro, tonalite, peridotite), and obtain a satisfactory fit of the friction evolution curves.

In section 5 we use the model to predict frictional evolution (a) at high slip rates and under normal load conditions corresponding to seismogenic depth (a combination of parameters so far impossible to match in laboratory experiments), (b) explore the general dependence of frictional parameters on normal stress and slip velocity and (c) how the extrusion of melt, or the absence thereof, alters the frictional behavior.

Section 6 compares the model behavior with field estimates from exhumed seismic faults.

Section 7 illustrates the behavior of friction assuming melting and a realistic slip-rate function (such that one would expect during an earthquake) with a time dependence more complex than a simple velocity stepping.

Section 8 is dedicated to a short discussion and conclusion, while in Appendix we describe some aspects of the numerical method and some details about the heat balance and the applied approximations.

2. Pre-melt phase and start of weakening

It is observed in high-velocity experiments that before bulk melting occurs, shear stress may oscillate but remains on average at a relatively high level (peak stress or τ_p) in the I.2
same range as the static Coulomb friction for rocks ($0.6\,\sigma_n < \tau_p < 0.7\,\sigma_n$). Our analysis of frictional melt applies to fault evolution after bulk melting has occurred, while pre-melt friction may be controlled by other processes such as flash heating at the asperity contacts [*Rice*, 2006; *Rempel and Weaver*, 2008; *Beeler et al.*, 2008], selective melting of minerals [*Shand*, 1916; *Spray*, 1992] or occurrence of melt at localized patches only [*Hirose and Shimamoto*, 2005; *Del Gaudio et al.*, 2009], which are well beyond the scope of this study. In addition, under normal stresses above of a few tens of MPa, experimental results indicate that the pre-melt oscillations tend to disappear and bulk melting occurs after an extremely short time lapse [*Nielsen et al.*, 2008; *Niemeijer et al.*, 2009]. Since such conditions of high normal stress are typical of faults at seismogenic depths, we may treat the pre-melt phase as a short episode of intense heat production under an approximately constant shear stress level τ_p. Assuming that frictional work rate $\tau_p V$ acts within an I.1
infinitesimally thin shear zone, and that heat diffuses perpendicularly from the shear zone, one may solve the 1D diffusion equation in order to estimate temperature evolution $T(t)$ [*Carslaw and Jaeger*, 1959] and to compute the time t_m at which melting temperature T_m is reached [*Cardwell et al.*, 1978; *Lachenbruch*, 1980; *Beeler*, 2006; *Nielsen et al.*, 2008,

Eq. 20, after correction of a misprinted factor 1/2], such that:

$$t_m = \pi\,\kappa\left(\frac{\rho\,c_p\,(T_m - T_i)}{\tau_p\,V}\right)^2 \tag{1}$$

$$\tau_p = \mu_s\,\sigma_n \tag{2}$$

where κ, ρ, c_p are diffusivity, mass density and heat capacity, respectively, T_m is bulk melting temperature of the rock, T_i initial temperature, μ_s a solid friction coefficient, σ_n normal stress and V the slip rate. In the above computation, it is assumed that $\tau_p\,V$ can II.5
be considered as a constant or as some representative average. We also remark that in the presence of pore fluid pressure P, the normal stress parameter σ_n should be replaced with an effective normal stress, i.e. $\sigma_n - P$, throughout this study. Finally, since we are dealing II.6
with polymineral rocks where parameters such as T_m, L and κ are slightly diefferent for each mineral, we define for simplicity a single bulk parameter for the whole rock assembly as a a ponderated average based on each mineral mass percentage.

After melting has occurred, we compute the viscous stress supported by the melt layer as described in the next section. Initially, the average melt thickness is arbitrarily thin, so that the stress supported by viscous shear could be virtually unbounded, while the strength of the rock is limited. As a consequence, we equate friction to the lowest of solid friction or viscous shear stress, and the apparent weakening takes on after a minimum growth of the melt layer has occurred, with a slight delay with respect to the time of melting.

3. Melt layer viscosity and thickness

This section describes frictional behavior after onset of melting.

We briefly recall the equations of the model derived in *Nielsen et al.* [2008], which remain mostly unchanged. In the present paper the same starting equations will be solved in a slightly more complex way involving numerical methods, because the transient case cannot be solved in closed analytical form.

The temperature diffusion equation needs to be solved both within the melt layer and within the solid rock bounding it on each side. Indeed the heat diffusion into the rock allows to evaluate the rate of melting while the temperature distribution within the melt allows to evaluate the viscosity (which is strongly dependent on both temperature and composition). As shown earlier [*Fialko and Khazan*, 2005; *Sirono et al.*, 2006; *Nielsen et al.*, 2008], the problem can be solved in 1D, neglecting heat transport and diffusion along directions other than perpendicular to the fault plane.

For practical reasons, we solve separately the problem of heat diffusion in the melt and that of heat diffusion into the solid, while the two solutions remain coupled through their mutual boundary: the melt/solid interface, where heat is exchanged and in part absorbed as a latent melting energy. I.3

We will first seek the solution of the heat diffusion inside the melt. After a continuous melt layer is formed, viscous shearing provides a source of heat rate $\tau\,\dot{\epsilon}(z)$ which is distributed unevenly across the melt (τ is shear stress and $\dot{\epsilon}$ is shear rate), resulting in inhomogeneous profiles of temperature, viscosity and shear rate across the layer. The resulting temperatures at the center of the melt layer can overshoot the melting temperature of several hundred degrees [*Nielsen et al.*, 2008]; as a consequence we cannot and do not make the approximation that the temperature is constant within the melt, in either transient or steady state regimes. We need to solve the heat equation in the form:

$$\frac{\partial T(z,t)}{\partial t} = \kappa \, \frac{\partial^2 T(z,t)}{\partial z^2} + v_z(z,t)\, \frac{\partial T(z,t)}{\partial z} + \frac{\tau(t)\, \dot{\epsilon}(z,t)}{\rho\, c_p}, \tag{3}$$

where the last term on the right-hand represents the heat source rate due to viscous shearing; v_z is the particle velocity in direction z, appearing in the transport term (second on the right hand side). I.4

The stress due to shear of a viscous fluid can be writen as $\tau(z) = \eta(z)\, \dot{\epsilon}(z)$ where η is viscosity, the slip rate V across the melt layer is $V = \int_{-\omega}^{+\omega} \dot{\epsilon}(z)\, dz$, and ω is the half thickness of the melt layer. Stress continuity implies that $\tau(z) = \tau$ is homogeneous across the layer, although shear rate $\dot{\epsilon}(z)$ is not. As a consequence we may write, in agreement with *Fialko and Khazan* [2005],

$$\tau = \frac{V}{\int_{-\omega}^{\omega} \eta(z)^{-1} dz} \tag{4}$$

If we define an equivalent shear viscosity η_s such that $\eta_s^{-1} = (1/\omega) \int_0^{\omega} \eta(z)^{-1} dz$ we obtain

$$\tau = \frac{\eta_s\, V}{2\, \omega} \tag{5}$$

The above relation is generally valid with no approximation for both transient and steady state, and no assumptions yet is made on the type of melt viscosity or its inhomogeneous distribution across the melt. I.5

Assuming that the temperature dependance of viscosity is governed by an Arrhenious law of the type $\eta = A\, \exp{(T_a/T)}$ (where T_a is a characteristic temperature) and using a linear approximation (the argument inside the exponential is replaced by its first order approximation in the vicinity melting temperature $T = T_m$) we obtain:

$$\eta(T) = \eta_c \exp -(T - T_m)/T_c \tag{6}$$

where $\eta_c = A \exp(T_a/T_m)$ and $T_c = T_m^2/T_a$ are constants with dimensions of Pa s and K, respectively. Since temperature, viscosity and shear rate are coupled and inhomogeneous, we need to seek conjunctly the solution for the viscosity profile $\eta(z)$ and for the temperature profile $T(z)$ within the melt layer, according to equations (3,4 and 6). We note that the effect of solid clasts in suspension in the melt, known to increase the viscosity value, is not explicitly included in this viscosity model. II.7

A particular approximate analytical solution for the profiles of temperature and viscosity inside the melt can be obtained [*Nielsen et al.*, 2008] by solving the boundary problem, under the assumptions that:

(I) The distributions of temperatures and heat sources within the melt layer are close I.7
to equilibrium - this does not exclude inhomogeneity and superheating above melting temperature, but only that time variations of the temperature within the melt are small with respect to other terms in equation (3). This leads to a valid approximation under transient conditions provided that the thermal diffusion within the melt layer is fast, so that the temperature profile is close to the equilibrium at any time. The typical rock thermal diffusivities are of the order of $\kappa \approx 10^{-6}$and the thickness of the melt in the experiments is of the order of 10^{-4}m, so that the thermal diffusion time ($t \propto z^2/\kappa$) across I.5b
the melt layer is extremely short, about 10^{-2}s , while the typical system latency (time required to evolve to a new equilibrium state) is regulated by the slower heat diffusion into the solid rock bounding the melt layer on either sides, which is of the order of $0.1 - 10$ s. As a consequence, it is reasonable to consider that the melt is always close

to thermal equilibrium in experimental conditions. For natural faults the observed melt thickness is more variable (even within a single fault) and can be larger. The field data I.5c of Tab. (3) reports indicative thickness measurements up to several millimeters but most indicate only a fraction of a millimeter. Detailed documented cases [*Sibson*, 1975; *Di Toro et al.*, 2005] describe how large proportions of the melt are extruded into side injection veins or extensional jogs, while effectively submillimeter-thin fault veins are found along contractional segments which should offer most of the frictional resistance to slip. Finally, melt at the beginning of slip, and during the intial transient, has not yet had time to build up to a consistent thickness, so that the approximation of thin melt is always true in the intial slip and for earthquakes with small slip amounts. As a consequence, we argue that the approximation should also hold to a good extent for cases of friction melt on natural faults, unless extremely large melt amounts are produced in the absence of an extrusion process.

(II) Within the melt, the power density τV produced by shear is large with respect to the balance of the heat rate due to net melt flow (heat carried in by new melt minus heat carried away by extruded melt). The heat balance and this specific assumptions are detailed in Appendix B, where numerical tests evaluate the accuracy of the approximation, concluding that it is viable in the parameter range discussed here. The approximate I.6 solution described in Appendix B leads to closed expressions for T and η within the melt layer of thickness 2ω $(-\omega < z < \omega)$ such that:

$$T(z) = T_m - T_c \log\left(\frac{\cosh^2\left(\frac{2\,z\,\tau}{\eta_c W}\sqrt{\frac{V^2}{W^2}+1}\right)}{\frac{V^2}{W^2}+1}\right) \tag{7}$$

$$\eta(z) = \eta_c \, e^{T_m/T_c} \left(\frac{V^2}{W^2} + 1 \right) \mathrm{sech}^2 \left(\frac{2\, z\, \tau \sqrt{\frac{V^2}{W^2} + 1}}{W\, \eta_c} \right) \tag{8}$$

where the characteristic rate W is defined by grouping the following parameters:

$$W = \sqrt{\frac{8\, T_c\, \breve{\kappa} \breve{\rho} \breve{c}_p}{\eta_c}}\, . \tag{9}$$

and $\breve{\kappa}$, $\breve{\rho}$, $\breve{c}$, refer to the thermal diffusivity, the mass density and the heat capacity, respectively (symbol $\breve{\cdot}$ refers to the parameters inside the melt). Finally, integration of (8) leads to the equivalent viscosity η_s :

$$\frac{1}{\eta_s} = \frac{1}{\omega} \int_0^{\omega} \frac{1}{\eta(z)}\, dz = \frac{V}{W\, \eta_c}\, \frac{\sqrt{\frac{V^2}{W^2} + 1}}{\mathrm{atanh}\left(\frac{V/W}{\sqrt{\frac{V^2}{W^2}+1}} \right)}\, . \tag{10}$$

Interestingly, the equivalent viscosity η_s only depends on slip rate V and fixed constitutive parameters; as a consequence, for fixed velocity the shear stress will vary only due to changes in thickness ω of the melt layer. The approximate solution (10) inside the melt hold for melt thicknesses of a fraction of a millimeter or less, and evolution times of seconds or more; for the study of a thicker melt layer or of a system evolving in shorter time intervals, it would be necessary to compute the value of η_s numerically.

We now focus on the diffusion equation in the solid, whose solution allows to compute the advancement rate ν of the melting front. This requires to solve the Stefan problem of heat diffusion inside the solid in the presence of a migrating boundary. In this case we may write the heat diffusion equation as:

$$\frac{\partial T}{\partial t} = \kappa\, \frac{\partial^2 T}{\partial \xi^2} + \nu\, \frac{\partial T}{\partial \xi} + \frac{\dot{q}}{\rho\, c_p}, \tag{11}$$

where ξ is the distance from the melt/solid boundary, while κ, ρ, c_p describe the thermal diffusivity, the mass density and the heat capacity inside the solid, respectively. Note that

we use ξ in (11) to make the distinction with position z in (4), where $\xi = 0$ corresponds to position $z = \omega$. Equation (11) assumes an Eulerian reference frame, attached to the melt/solid boundary, which advances at velocity ν into the solid. Unlike the steady state case studied by *Nielsen et al.* [2008], the shortening rate ν is variable and Eq. (11) needs to be solved numerically, as explained in the Appendix A. The term $\dot{q}$ represents possible additional heat sinks or sources other than frictional heating or latent heat. We use it to account for convective exchange (advection into the air at sample boundaries, also known I.8
as Newtonian radiation condition, see Appendix A) by contact between the air and the outer border $r = R$ of the cylindrical sample used in the experiment.

The melt boundary velocity ν depends on the rate of melting, hence on the balance between latent heat L and Fourier heat flow leaving or entering the boundary, toward solid side ($\xi = 0^+$) or melt side ($\xi = 0^-$), respectively:

$$\begin{aligned} \rho\, L\, \nu \;&=\; \kappa\, \rho\, c_p \left.\frac{\partial T}{\partial \xi}\right|_{0^+} \;-\; \breve{\kappa}\, \breve{\rho}\, \breve{c}_p \left.\frac{\partial T}{\partial \xi}\right|_{0^-} \\ &\approx\; \kappa\, \rho\, c_p \left.\frac{\partial T}{\partial \xi}\right|_{0^+} \;+\; \frac{\tau\, V}{2}\,. \end{aligned} \tag{12}$$

In light of the typical orders of magnitude expected for the flow rate and temperature gradients inside the melt, we have assumed that most shearing heat rate $\tau\, V$ produced in the melt enters the boundary, and used the approximation $\partial T/\partial \xi|_{0^-} \approx -\tau\, V/(2\, \breve{\kappa}\, \breve{\rho}\, \breve{c}_p)$ as discussed in *Nielsen et al.* [2008] and also in Appendix B. The factor of 2 accounts for the presence of two boundaries (one on each side of the melt layer).

The term $\frac{\partial T}{\partial \xi}|_{0^+}$ in eq. (12) is obtained by solving of eq. (11). It represents the heat flow diffused into the solid. Thus (11) and (12) clearly form a non-linear system of two coupled equations: ν appears in both equations and $\frac{\partial T}{\partial \xi}|_{0^+}$ is a result from (11) when $\xi \to 0^+$. II.8

Once the melting/freezing rate ν is obtained by solving (11, 12), we need to define an extrusion mechanism in order to compute the rate of melt extrusion. To this purpose we follow the approach of *Nielsen et al.* [2009] regarding normal stress and evolution of the melt layer thickness, taking into account the roughness of the melt/solid interface. *Nielsen et al.* [2009] consider shear of a melt layer in the slipping zone but with a partial contact at isolated asperities, and derived a normal stress in the form:

$$\sigma_n = (1 - \alpha) \frac{C \, \eta_e \, \dot{\omega}_c \, R^2}{\omega^3} + \alpha \, \sigma_c \, . \tag{13}$$

where α is the ratio of asperity contact area versus total area and $\dot{\omega}_c$ is the rate of I.9 squeezing, or the amount of extruded melt per unit fault surface and time. Extrusion I.11 (squeezing) is controlled by the outer radius of the sample and by the inner radius, too, in case of annular samples [*Fialko and Khazan*, 2005; *Nielsen et al.*, 2008]. However, on natural faults the extrusion, if any, is controlled by the mean length of flow of the melt before it encounters an extrusion vein or a distensional jog. In this case, the squeezing I.12 process may still be described by Eq (13) but departure from a cylindrical symmetry will alter the value of the geometrical constant C, and the significance of the mean length of flow R needs to be defined depending on the natural fault structure. Eventually, on faults with very unfrequent veins or pooling sections, the situation may be expressed by $R \rightarrow \infty$, which is equivalent to a situation of no extrusion. The absence or the limitation of extrusion, and their effects on friction, will be further discussed and modeled in section 5.

As of Eq. (13), the applied normal stress σ_n is partitioned into a viscous pressure term and a contact stress term resulting from contact asperities in a state of incipient plastic flow, where σ_c is the indentation hardness. Since minerals in the vicinity of the sliding interface are at temperatures approaching the melting point, we adopt values of σ_c much lower than the nominal values at ambient temperature (see Table 1). Assuming that the melt/solid boundary has a small-scale topography of dominant elevation ω_0, the partition term α can be described by [*Nielsen et al.*, 2009]:

$$\begin{aligned} \alpha(\omega) &= \tfrac{\omega_0^2}{\omega^2}\, e^{-\frac{\omega^2}{2\,\omega_0^2}} \\ \alpha(\omega) &\leq \sigma_n/\sigma_c\,. \end{aligned} \tag{14}$$

In addition, the dominant elevation ω_0 evolves as the inverse of the temperature gradient

$$\omega_0 \approx \frac{1}{2}\Delta T \Big/ \left.\frac{\partial T}{\partial z}\right|_{0^+} \tag{15}$$

due to preferential melting, where ΔT is of the order of the difference in melting temperature between the mineral constituents of the wall rock and $\left.\frac{\partial T}{\partial z}\right|_{0^+}$ is, again, the temperature gradient in the solid in the immediate vicinity of the melting boundary obtained by the solution of (11).

Finally, we may use at any time t the differential equation defining the rate of thickening obtained in *Nielsen et al.* [2009]. The melt layer thickness results from the competing mechanisms of melt production and extrusion (if extrusion is present), or the concurring mechanisms of melt freezing and extrusion. We may write:

$$\begin{aligned} \dot{\omega}(t) &= -\mathcal{H}\left(\dot{\omega}_c(t)\right) + \nu(t) \\ \omega(t) &= \int_0^t \dot{\omega}(t')\, dt' = \sum_{n=1}^{N} \dot{\omega}(n)\, \delta t\,, \end{aligned} \tag{16}$$

where $\dot{\omega}$ refers to the time derivative of the average melt thickness while $\dot{\omega}_c$ is the rate of squeezing alone (extruded melt per unit fault surface and time). $\mathcal{H}$ is the Heaviside step function, introduced to avoid negative squeezing rates, under the assumption that melt cannot return once extruded.

If the extrusion is effective (like in the unconfined laboratory experiments and in the natural faults with numerous injection veins on the fault sides) a steady state is reached where extrusion and melting compensate each other and the melt thickness remains constant. However, while extrusion condition is inevitable in experiments, it may not always II.2 be met on natural faults [*Sirono et al.*, 2006]. In the present study we will use the modeling technique in order to predict the behavior of frictional melt in the absence of extrusion (see section 5, Fig. 8 and Fig. 10), thus extrapolating laboratory results. During cooling stages melting process is converted into a freezing process, so both extrusion and freezing will concur in reducing melt thickness.

In the experiments, extrusion induces a measurable convergence rate of the two opposite samples equal to $2\dot{\omega}_c$ provided that the melting expansion of the rock is negligible.

Time iteration of the equation system (5-16) is essentially the solution to the frictional melt problem. The only numerical solutions required are that of (11), described in Appendix A, and the simple time extrapolation of thickness in eq. (16).

4. Modeling of experimental results

We compare results from the theoretical and numerical model developed in section 3 with a number of mechanical data from frictional melt experiments, for different types of rocks (gabbro, tonalite and peridotite), under various normal stress (σ_n =0.8-15 MPa) and slip velocity (V = 0.8-1.4 m/s) conditions, including experiments where velocity steps are applied.

For each rock type, we fix the heat capacity c_p, latent heat L, mass density ρ and melting temperature T_m, indentation hardness σ_c and diffusivity κ according to standard values (see Table 1). We use relatively low heat diffusivity value κ, to account for the substantial diffusivity drop observed in rock-forming minerals in the vicinity of melting temperatures [*Whittington et al.*, 2009]. We also fix an indicative value for the variability of melting temperature ΔT to account for inhomogeneities of the rock [*Nielsen et al.*, 2009], and include a slight heat loss H (see Appendix A and Table 1) to account for Newtonian radiation at the contact of the air. Finally, we seek for the best combination of the two parameters controlling the viscosity law in the melt, W and η_c, fitting all the experiments for a given rock type. The resulting fit is represented in figures (1-5). I.10

The general observation for all these simulations of experiments, is that the variations in the duration of the initial transient in the presence of a layer of melt, the relative friction decay and the velocity dependance (at least during the steady velocity intervals) are all accurately reproduced by the model, within the range of different normal stresses and slip velocities imposed, using the same parameter set (diffusivity, density, viscosity law parameters, etc) for each rock category.

One feature that appears to be variably well reproduced is the final restrengthening (friction recovery) episode when the slip-rate decreases to zero. The misfit is particlarly noticed in Fig (1) where no apparent restrengthening is observed in the experimental data. Since generally restrengthening is observed in frictional melt experiments, it is possible that this particular experiment was problematic, in particular, due to the fact that the sample used was a solid cylinder in order to support the high normal stress imposed with a reduced risk of destroying the sample. It was observed after several solid cylinder experiments that the final shape of the sample was meniscus-like or arched, so that the central protruding section supported most of the normal load and prevented efficient squeezing and melt extrusion from the borders of the sample towards the end of the experiment. As commented in section 5 and Fig. (8), preventing extrusion considerably reduces the restrengthening effect in the decelerating phases.

Other striking discrepancies in the restrengthening are found mainly in Fig. (3) and (4). In (3), while restrengthening is marked in both experimental and modeled stress curves, we note an overestimate of the modeled restrengthening with respect to the experimental data, in particular, a larger final friction. This may be due to the inertial effect of the machine rotation which is not modeled here. The inertial aspect results in the arrest of slip at variable shear stress levels, depending on how rapidly the kinetic energy of the rotating machine parts is dissipated by the friction on both the sample and the machine ball bearings. This inertial effect is described to some length in *Del Gaudio et al.* [2009] and we do not restate the discussion here. However, we note that in general the inertia of the machine is fully dissipated and slip stops somewhat abruptly before the friction is able to fully recover on to its maximum possible value on the sample. The model does not account for such an inertial effect and thus slip continues until the maximum recovery is reached. In Fig. (4), the sample partly failed prior to the deceleration (bumpy curve from the 9th second on) , so that the friction recovery process monitored in the experiment is not reliable.

Finally, we also show in the example of Fig (6) the comparison between experimentally measured shortening of the sample and the value obtained in the model as a function of time, as well as the model results for melt thickness and maximum temperature (super-heating above melt temperature).

In general, we note that, while the general features and trends of the experimental transient are well reproduced by the model, the limited range of experimental values yet available and the problems related to the sample reduced size and mechanical limitations of the experimental machine, prevent a very detailed comparison between the data and the model behavior.

5. Modeling of Earth seismogenic conditions

In this section we discuss the general trends of the frictional behavior, in terms of how much time, slip and energy dissipation are necessary to achieve weakening under various conditions of normals stress and slip velocity. For simplicity, we first keep the radius of extrusion constant at $R = 1$cm and later in this section comment specifically on the effect of increasing the extrusion radius to $R = \infty$ effectively modeling cases where no extrusion is allowed.

Also note that throughout this work we assumed constant or step-wise constant slip velocity, which is an oversimplification of what occurs during an actual earthquake. The precise evolution of friction expected under an impulse of highly variable slip velocity associated with the earthquake rupture is not discussed here. However the presented results are indicative of the main frictional features expected for faults that are seated deep in the Earth crust (considerably increasing the normal stress beyond the available experimental range) and increasingly preloaded (inducing higher slip rates). In addition, the characterization of friction should help to design a constitutive law in the framework of frictional melt and, optimistically, that of several thermal weakening processes that may occur on seismic faults (decarbonation, dehydration, gelification,...).

We investigate how some key friction parameters such as breakdown energy, slip weakening distance and weakening time evolve when normal stress and slip velocity are altered.

For clarity, we begin by stating precisely the definition that we adopted here for such parameters .

We define the breakdown energy W_b as the energy dissipated by the friction in excess of τ_{ss}: I.13

$$W_b = \lim_{U \to \infty} \int_0^U (\tau - \tau_{ss})\, du \tag{17}$$

where U is slip (for a seismological definition see *Tinti et al.*, 2005). The above limit is defined provided that τ_{ss} exists (for frictional melt with extrusion, the existence of a steady state was shown in *Nielsen et al.*, 2008) and W_b can be satisfactorily estimated at finite U. For compatibility with the definition provided in seismological estimates of breakdown work [*Tinti et al.*, 2005], we have defined W_b at infinite slip (where it is assumed that τ_{ss} is a minimum value in some sense). This is also the approach advocated in *Beeler* [2006] for estimating W_b from laboratory experiments. In nature, seismological estimates yield I.14
W_B ranging from 1 to 80 MJ/m^2 for moderate to large size earthquakes [*Abercrombie and Rice*, 2005; *Tinti et al.*, 2005; *Cocco and Tinti*, 2008; *Tinti et al.*, 2009].

Moreover, we define the thermal weakening time t_{th} as the time necessary to obtain a significant weakening under given conditions of slip velocity and normal stress, where significant weakening corresponds to a partial friction drop of about 0.63 (or $1 - 1/e$) of the total drop. As a consequence, we define t_{th} as the time when

$$\tau = \tau_{ss} + (\tau_p - \tau_{ss})/e \tag{18}$$

Finally, we define the thermal weakening distance D_{th} as the amount of slip at which eq. (18) is verified. In the case that $V = Const$ we may write $D_{th} = t_{th}\, V$.

For the definition of all of t_{th}, D_{th} and W_b we do include the initial slip plateau under a constant Coulomb stress. In order to compute their arithmetical values, we run numerical simulations until the frictional variation rate is negligible and an apparent steady state is reached. Assuming an exponential decay, the difference between the steady state value and an the actual value of friction is less that 0.7% for $U \geq 5\,D_{th}$.

Different combinations of normal stress and velocity were explored ($V =$ 1, 3, and 9 m/s; $\sigma_n =$ 1, 2, 3, 8, 16, 32 and 64 MPa). Given that the shear stress peak values in the initial part of the transient are proportional to the normal stress in agreement with a Coulomb friction law, followed by a quasi-exponential decay from peak to steady state, it follows that the shear stress during the whole transient scales with normal stress [*Nielsen et al.*, 2008]; we may write $\tau(t) = \mu\,\sigma_n\,f(t)$ where $f(t)$ is a dimensionless function describing the time evolution of the friction. The heat density at the sliding interface results from the time integral of the imposed heat flow, $\tau(t)\,V(t)/2$, divided by the square root of time, according to classic heat diffusion solutions (*Carslaw and Jaeger*, 1959):

$$\begin{aligned} T_v(t) - T_i &= \frac{1}{\rho\, c_p \sqrt{\kappa\,\pi}} \int_0^t \frac{\tau(t-\xi)\,V(t-\xi)}{2\sqrt{\xi}}\,d\xi \\ &= \mu\,\sigma_n\,V\,\frac{1}{\rho\, c_p \sqrt{\kappa\,\pi}} \int_0^t \frac{f(t-\xi)}{2\sqrt{\xi}}\,d\xi \end{aligned} \qquad (19)$$

where $T_v(t) - T_i$ represents a virtual temperature increase that would have been reached at the interface in the absence of heat sinks such as latent heat, radiation loss, etc.... It follows that the heat density and temperature at the interface both scale with $\sigma_n\,V$ and, given that melting is a thermally activated process, we expect the duration of the frictional transient to scale somehow with the inverse square of power density $1/(\sigma\,V)^2$. On the other hand, the slip distance during a given time interval is proportional to slip velocity V, so that we expect the thermal weakening distance D_{th} to scale as $1/(\sigma_n\sqrt{V})^2$. Similar dimensional arguments for the dependance of D_{th}, t_{th} based on heating have been discussed in other contexts than frictional melt by *Beeler* [2006], and by *Brantut et al.* [2008].

Indeed we find that the data points collapse on a single curve when represented as a function of $\sigma_n\, V$ for all parameters except for D_{th}which collapses for $\sigma_n\,\sqrt{V}$ (Figure 7).

Finally, the steady state stress τ_{ss} should scale as $((\sigma_n - \alpha\,\sigma_c)/(1-\alpha))^{1/4}$ (Eq. 13 and *Nielsen et al.*, 2009). However, neglecting α at high slip rates and normal stress, the scaling can be assimilated to $\sigma_n^{1/4}$. As an approximation to a complex velocity-dependence, as some negative power of slip rate V as shown by *Nielsen et al.* [2008]. Figure 7-(c) shows the collapsing data of steady state shear stress as a function of σ_n/V , indicating a good fit with a slope of 1/4 compatibly with the analytical solutions [*Nielsen et al.*, 2008, 2009] and with experimental observations (within the limit of those available now). The experiments and the models performed under relatively low slip rates (V≈1m/s) show a departure from the general trend because the effect of α (Eq. 13) on the normal stress is not negligible.

These trends, in particular the dependence on the effective slip-weakening distance with normal stress and with velocity, are compatible with peridotite behavior under high velocity slip as described by *Del Gaudio et al.* [2009].

Finally, the breakdown energy W_b is virtually independent of both normal stress and slip rate. Indeed, while the initial amplitude of stress is proportional to σ_n, the duration of the weakening transient is inversely proportional to σ_n, so the effect on duration and amplitude in the area under the stress-slip curve defining W_b roughly compensate each other. On the other hand, faster slip rates tend to decrease the slip weakening distance as $1/\sqrt{V}$, so the area W_b should slightly decrease with velocity. Overall the variations of W_b are negligible. This point is crucial because W_b is one of the few dynamic parameters which one expects to effectively constrain from seismic data of earthquakes [*Tinti et al.*, 2005], while D_{th} and τ_p are difficult to resolve independently. For example, no significant variation of W_b with depth should be observed in seismic data for faults that undergo melt, although frictional behavior is expected to change with lithostatic load, because the resulting W_b is for all practical purposes independent of normal stress.

An illustration of the extrusion radius effect is proposed in Fig. 8. The effect of increasing the radius of extrusion R (a) delays the onset of steady state, until no steady state is reached for $R \to \infty$ and (b) limits the rapid recovery of stress in the final stage of slip where the slip velocity is decreasing. A consequence of (b) is that generation of short slip pulses will happen more easily for relatively small extrusion radii, or equivalently, on natural earthquake faults, for injection veins and melt pools at dilation jogs that are not more than a few centimeters apart.

In conclusion, frictional behavior parameters for earthquake faults with a thermally activated behavior, in general, and for frictional melt in particular, may behave as a function of lithostatic load and slip velocity as illustrated in (Figure 7), with a decreasing slip weakening distance and weakening time when both V and σ_n increase and with a dramatic lubrication effect in the steady state friction. However the breakdown energy is only weakly dependent on normal load, owing to its opposite effect on transient duration and on initial peak stress. Finally, rapid frictional recovery when slip rate is decelerating is found, a feature which is enhanced when the extrusion radius R is relatively small (a few cm). We may sum up the resulting frictional behavior in the following trends:

$$\begin{array}{rcl} t_{th} & \propto & (\sigma_n V)^{-a}\,(1/2 < a < 2) \\ D_{th} & \propto & (\sigma_n \sqrt{V})^{-a} \\ \tau_{ss} & \propto & (\sigma_n/V)^{1/4} \\ W_b & \approx & \text{Const.}\,(1-10\,\mathrm{MJ/m^2}) \end{array} \tag{20}$$

We briefly comment on the above results. First we discuss the thermal weakening time t_{th}, which is related to heat production rate and similarly the thermal weakening distance D_{th}. We may assume that weakening, in our case, is achieved when the formation of a low-viscosity film of melt is completed [*Fialko and Khazan*, 2005; *Hirose and Shimamoto*, 2005; *Del Gaudio et al.*, 2009]: this occurs when the temperature reaches or surpasses a given threshold throughout a finite thickness of material. During the very initial slip stages before pervasive melting occurs (see for example first 2 sec. in Fig. 2), both the measured peak friction [*Del Gaudio et al.*, 2009] and the average friction level are matched by a Coulomb law ($\mu\,\sigma_n$). Hence heat production rate is initially proportional to $\sigma_n V$, temperature should rise like $\Delta T \propto \sigma_n V \sqrt{t}$ [*Carslaw and Jaeger*, 1959] and time to reach a given temperature threshold scales with $(\sigma_n V)^{-2}$. Similar scaling arguments I.16 based on temperature rise were proposed before [*Beeler*, 2006; *Brantut et al.*, 2008; *Nielsen et al.*, 2008]; however in the final stages of weakening, friction tends to the steady state residual value $\tau_{ss} \propto (\sigma_n/V)^{1/4}$, implying a heat production rate in $\sigma_n^{1/4} V^{3/4}$ and a time for temperature rise which should scale in $\sigma_n^{-1/2} V^{-3/2}$. As a consequence there is no simple way to characterize the temperature rise through the whole duration of the weakening interval.

For experiments with relatively low heat production rate ($1 < \sigma_n V < 50\,\mathrm{MW/m^2}$), the pre-melting phase lasts for up to several seconds and tends to dominate the weakening interval with an average heat rate close to$\mu\,\sigma_n V$. Indeed, t_{th} shows a scaling with $(\sigma_n V)^{-a}$

with $a = 2$ in the left part of the graphic (Fig. 7-a). Under the same conditions, the thermal weakening distance D_{th} shows a scaling in $(\sigma_n \sqrt{V})^{-2}$, which may be predicted by straightforward multiplication of t_{th} with V (Fig. 7-b). However, as $\sigma_n V$ increases the pre-melt stage becomes extremely short; in the whole weakening time interval, the initial stage with heat rate proportional to $\sigma_n V$ becomes less dominant. This alters the dependance of both t_{th} and D_{th} and the scaling in Fig. (7-a) of (σ_n, V) is non-trivial. We note that the general trend is compatible with a dependence in $(\sigma_n V)^a$ for t_{th} and in $(\sigma_n \sqrt{V})^{-a}$ for D_{th} with, on average $a \approx -1$ (at lower values of $\sigma_n V$ the exponent is closer to -2, and closer to -1/2 at higher values).

Furthermore, the steady state τ_{ss} is compatible with the previous analytical predictions in $\sigma_n^{1/4} f(V)$, although, for simplicity, the complex velocity dependence function $f(V)$ derived in [*Nielsen et al.*, 2008] may be replaced with $V^{-1/4}$.

Finally, we comment on the breakdown energy W_b, which corresponds to the integral of the slip-shear stress excess curve during the weakening stage (see definition in Eq. 17) and we may write $W_b \approx (\bar{\tau} - \tau_{ss})\, D_{th}$ where $\bar{\tau}$ is a the average friction during the weakening. From the above discussion, we may consider that an increase in either normal stress or slip rate will reflect in a increase of $\bar{\tau}$ but in a decrease of D_{th}, inducing, on the two main factors controlling W_b, antagonistic effects which seem to counterbalance each-other leaving an essentially constant breakdown energy.

6. Comparison with field data

Coseismic friction during ancient earthquakes can be estimated on exhumed faults bearing solidified frictional melt (i.e., pseudotachylites: *Sibson*, 1975; *Di Toro et al.*, 2006a, b). We present a synthesis of data collected on exhumed seismic faults recently surveyed in the Outer Hebrides, Scotland, and merge them with measurements from (*Sibson*, 1975) obtained on the same fault zone. The thrust faults were at depths of about 10 km at time of seismicity and they cross-cut quartzo-feldspathic gneisses, with similar mineral composition and thermal properties as tonalite (see Table 1).

Separation markers were visible on the exposed surfaces; assuming that the measured separation approximately coincides with co-seismic slip U, it is possible to relate the amount of co-seismic slip to the pseudotachylite thickness and to the average dynamic friction level $\bar{\tau}$ estimated on each of the documented faults, according to the equation:

$$\bar{\tau} \approx 2\omega\, E\, \rho / U \tag{21}$$

[*Sibson*, 1975; *Di Toro et al.*, 2006a, b], where $E = L(1-\phi) + c_p(T_m - T_i)$ is the energy required to produce a kg of melt and ϕ is the portion of surviving mineral clasts in the melt Assuming that slip on all faults took place under similar average conditions of slip- I.18
rate and lithostatic load, the assemblage of data from faults with different slip amounts (data reported in Table 3) is used to illustrate the progressive frictional decay versus slip in Fig. (9). A clarification is improtant here: since the amount of melt produced on faults is related to the integral of frictional work within the whole slip episode, it follows that the stress amount resulting from Eq. (21) corresponds to the average of the stress curve up to the measured slip, rather than to the value of the stress reached at the measured amount of final slip. As a consequence, it is important to note that the direct result of Eq. (21) is not the actual stress vs. slip curve but rather an overstimate of the latter, in particular for values belonging to the initial transient.

For the sake of comparison with the model, we simulate frictional evolution according to the model of section 3 assuming an effective normal load of $\sigma_n \approx$200MPa (corresponding to a lithostatic load at 10 km depth and hydrostatic pore pressure conditions), an average slip rate of $V = 1\,\mathrm{m/s}$ (a representative value for seismic slip rate). Since the mineral composition of the observed quartzo-feldspathic gneiss is very similar to that of a tonalite, we use the same rock constitutive parameters as in Table (1). From the numerical results, we compute the average friction $\bar{\tau}$ within different time intervals corresponding to increasing slip amounts from 0.015 m (slip necessary to achieve melting under the imposed conditions) and 2 m (about the maximum separation measured in the field). Finally we can compare the friction decay obtained from the model and from the field estimates. Both are represented in Fig. (9).

Since there are no clear markers of slip direction on the outcrop, the exposed surface may not be perfectly parallel to the slip direction. As a consequence the separation measurements may yield either an under- or an overestimate of the actual co-seismic slip on the faults, as this reflects in the relative scatter of the data in Fig. (9). In addition, conditions at time of seismicity are not altogether well constrained. In spite of all this, one expects the field estimates of friction and decay distance to fall in a representative order of magnitude. Effectively the model and the measurements show satisfactory similarities within the limits of the scatter and uncertainties.

An outcome of this synthesis from model and field data, is that the order of D_{th} is a few cm and that of residual shear stress is of a few tens of MPa ($\mu \leq 0.1$) at 10 km depth and in the presence of friction melts.

7. Toward a rate-and-state formulation of frictional melt

While existing rate-and-state friction laws are suitable to describe slow slip during interseismic phases or earthquake nucleation, it is recognized that they cannot be extrapolated as-is to the fast slip conditions during the dynamic earthquake slip. However, generalized rate-and-state equations could be designed which also fit the dynamic friction conditions and, in particular, the behavior of frictional melt, for convenient use in earthquake modeling techniques. II.3

The experimental trends described in section 5 are indicative and hold under the assumption that slip rate can be considered as a constant or as a significant average, a condition often imposed in rock friction experiments. In addition they are but approximations of a more subtle and complex behavior; we note for example that Eq. 20 works as an approximation to the slightly more complex velocity dependence predicted by the analytical solution of *Nielsen et al.* [2008] or that obtained by the complete solution of section 3.

It is clear that the high velocity friction of melting surfaces depends on the previous sliding history in a non-trivial, irreversible manner. During an earthquake the slip rate is highly variable in time. In such case the full solution of section 3 should be used. Although many recent laboratory tests are based on simple velocity-stepping precedures, *Del Gaudio et al.* [2009] investigated stress recovery during the decelerating stage and *Sone and Shimamoto* [2009] illustrated the effect of a more realistic slip rate pulse applied to samples in high velocity rock friction experiments. We propose here an example where the imposed slip history is highly variable and mimics the slip acceleration expected at a point on a fault during dynamic fracture, and compute the friction evolution according to the full solution as of section 3.

We imposed slip corresponding to a dynamic self-healing rupture pulse of the form of a Yoffe function $V = \mathrm{Re}[\sqrt{t_h - t}/\sqrt{t - t_f}]$ obtained by analytic solution [*Nielsen and Madariaga*, 2003], with a total rise time $t_h - t_f = 5\,\mathrm{s}$. The function was smoothed in order to remove the initial singularity (using a Gaussian moving average of with standard deviation of 0.2 s) resulting in an initial ramp of about 0.6 s (see Fig 10). The friction was computed for extrusion radii R $= 1\,\mathrm{cm}$ and R $= \infty$, under either $\sigma_n = 10\,\mathrm{MPa}$ (Fig 10-a) or $\sigma_n = 64\,\mathrm{MPa}$ (Fig 10-b). In all cases the weakening is very fast and there is considerable hardening as the slip rate drops in the later part of the slip function. Friction increases to static values even before slip rate is zero. This increase in friction I.19 is an efficient mechanism to promote self-healing pulses in dynamic rupture [*Zheng and Rice*, 1998; *Nielsen and Carlson*, 2000; *Nielsen and Madariaga*, 2003; *Lu et al.*, 2007].

For use in dynamic seismic source models, this type of solution for melting with heat diffusion could be computed at each point of a discretized fault, in order to derive the time evolution of the friction, coupled to a 3D elasto-dynamic solution of the wave equation. However, the resulting computation would be probably cumbersome and numerically costly.

In alternative, future efforts should be dedicated to finding a general mathematical formulation in the framework of rate-and-state laws, in order to describe frictional melt (and in general high velocity friction). Some aspects of the friction evolution law are described empirically by *Sone and Shimamoto* [2009] although non-linear dependence of the parameters on normal stress and sample dimensions (e.g. extrusion radius) is not accounted for. The rich variability of the parameters upon normal stress, extrusion radius and slip rate, combined to the elusive irreversibility character (due temperature rise and phase transitions) of frictional melt, requires a fundamental reformulation of the existing rate-and-state laws which describe friction under relatively slow, aseismic slip rate. The main difficulty consists in mimicking with state equations, the evolution of heat diffusion with a migrating boundary and its interplay with the melt layer.

8. Conclusions

We develop a physical model describing friction at high velocity in the presence of heat diffusion, melting, viscous shearing of a melt layer with inhomogeneous viscosity and extrusion of melt. The model reproduces satisfactorily features observed in a wide range of experimental conditions and is in agreement with qualitatively estimates from field measurements on ancient pseudotachylite-bearing seismic faults.

We then use the frictional model in order to extrapolate experimental results to conditions expected in the real Earth. We proceed to show the general trends of slip weakening, weakening time, breakdown energy and steady state stress when the normal stress and the slip velocity vary; examples of changing the extrusion radius for the melt are shown. Finally, examples of friction evolution when a realistic time-function of slip is imposed. The latter examples show a strong restrengthening in their later phases of the slip (when slip rate is dropping), which is known as an important ingredient for promoting self-healing of dynamic ruptures.

The full solution of the problem requires a numerical scheme for the 1D diffusion equation with a moving boundary, which is ideally possible to use in dynamic rupture fault models but may result in a rather cumbersome and inefficient computation. In future studies effort should be dedicated to finding a more compact formulation, in the framework of rate-and-state laws, mimicking the main features of high-velocity frictional evolution and its dependence on ambient conditions.

Appendix A: Numerical solution of the diffusion problem

We solve numerically eq. (11) representing thermal diffusion in the presence of a boundary moving at velocity ν (where ν is computed according to 12). For 1D solutions we adopted a finite difference scheme of second order in space using the Crank-Nicholson method for time updating [*Crank and Nicolson*, 1947]. An incoming heat flow $\tau V/2$ is imposed at the boundary $\xi = 0$ of the model (see Appendix B for details on boundary conditions and heat balance) and a minor heat sink is added to account for loss through air contact (see below).

We account for Newtonian radiation by contact between air and the outer border $r = R$ of the sample. The heat loss rate through the outer border of an object, per unit surface, is generally modeled through an empirical constant H (coefficient of convective exchange, in m^{-1}) such that (*Carslaw and Jaeger*, 1959):

$$\dot{q} = \kappa\,\rho\,c_p\,\frac{\partial T}{\partial r} = -H\,\kappa\,\rho\,c_p\,(T_{int} - T_{ext}) \tag{A1}$$

Where T_{int} is the average inner temperature of the body and T_{ext} is the air temperature. In a cylindrical disk of elementary height dz and radius R the exposed surface is $2\,\pi\,R\,dz$. Assuming that an average temperature $T_{int}(z,t)$ is present at height z inside the sample, the associated heat loss rate for each disk dz is:

$$\dot{Q}(z,t) = 2\,\pi\,R\,dz\,\dot{q}(z)$$
$$= -2\,\pi\,R\,dz\,H\,\kappa\,\rho\,c_p\,(T_{int}(z,t) - T_{ext}). \tag{A2}$$

We do apply the above heat loss at each node of our 1D simulation, as an approximation to the fully cylindrical solution with a boundary condition.

In order to check whether the 1D solution is compatible with the actual geometry of the high velocity rotary friction experiments, we performed 2D simulations reproducing the shape of the cylindrical samples, allowing for more realistic boundary conditions. The numerical problem was solved using a Peachman and Rachford scheme [*Peachman and Rachford*, 1955]. In this case the heat loss at air contact was applied explicitly at the outer radius of the sample. The heat flow imposed at the sliding boundary of the sample ($\xi = 0$) was inhomogeneus in order to account for the radial dependance of slip velocity $V(r) = \dot{\theta}\,r$ (where $\dot{\theta}$ is the angular velocity of the rotating sample), resulting in the incoming heat flow $\tau\,\dot{\theta}\,r/2$ (as opposed to the average heat flow $\tau\,V$ based on the equivalent velocity V). The relationship between the angular velocity $\dot{\theta}$, sample outer radius R and the equivalent linear velocity V are described elsewhere [*Hirose and Shimamoto*, 2005; *Nielsen et al.*, 2008]. The complete cylindrical simulations (not shown here) and the 1D solution showed shear stress evolution results that were largely compatible. In both cases, the implementation of heat loss at the sample border (using Eq. A2 in the 1D approximation) induce a more rapid convergence toward the steady state, eliminating a long-term slow evolution of the shear stress otherwise present in the simulations, but not in the experiments.

Appendix B: heat balance and power density approximation

We discuss here some aspects of the heat balance and the approximations done. A closed analytical solution can be obtained for the temperature and viscosity profiles within the melt, provided that the deat diffusion Eq. (3) is reduced to the following form:

$$\frac{\partial^2 T}{\partial z^2} = -\frac{\tau^2 \exp\left(T(z)/T_c\right)}{\eta_c \breve{\kappa} \breve{\rho} \breve{c}_p \exp(T_m/T_c)} \tag{B1}$$

This simplified equation results when adopting a temperature dependence of viscosity in the form $\eta(T) = \eta_c \exp\left(-(T - T_m)/T_c\right)$ and replacing it in the shear heating source term of Eq. (3) such that $\dot{\epsilon} = \tau/\eta(T(z))$. In addition, the heat source term is considered as dominant in Eq. (3) with respect to time variation term $\partial_t T$ (the melt is always close to equilibrium because it is thin, or assumption I) and with respect to the transport term $\nu \partial_z T$ (the upper bound of the Peclet dimensionless number $\nu\omega/\kappa$ is 0.1, *Nielsen et al.*, 2008) so that the two latter terms are neglected.

The solution of Eq. (B1) requires two boundary conditions, namely, both the temperature and the temperature gradient at the boundary of the melt toward the melt, i.e. $z = \omega^-$. The first condition is straightforwardly that $T(\omega) = T_m$, i.e., melting temperature at the boundary. The second condition, on temperature gradient, requires some considerations on the thermal balance as described below.

For simplicity, we consider three different entities, solid, and melt and the boundary between the two. The heat gains and losses for each of them may be described in the following terms, where ν and $\dot{\omega_c}$ are defined as positive for rates of melt advancement and extrusion, respectively, such that within each given compartmnent (solid, melt, boundary) a term with minus sign represents a heat loss and a term with a plus sign a heat gain, per unit time and per unit fault surface:

$$
\begin{aligned}
&\text{solid :} && \begin{cases} \text{outflow to melt} & -\rho\, c_p\, \nu\, (T_m - T_i) \\ \text{diff. heat inflow} & +\kappa\, \rho\, c_p\, \left.\frac{\partial T}{\partial z}\right|_{\omega^+} \end{cases} \\
&\text{melt :} && \begin{cases} \text{melt inflow} & +\breve{\rho}\, \breve{c}_p\, \breve{\nu}\, (T_m - T_i) \\ \text{melt extrusion} & -\breve{\rho}\, \breve{c}_p\, \dot{\omega}_c (\bar{T} - T_i) \\ \text{diffu. heat outflow} & -\breve{\kappa}\, \breve{\rho}\, \breve{c}_p\, \left.\frac{\partial T}{\partial z}\right|_{\omega^-} \\ \text{shear heating} & +\tau\, V/2 \end{cases} \\
&\text{boundary :} && \begin{cases} \text{latent heat} & -\breve{\rho}\, \nu\, L \\ \text{diffu. heat outflow} & -\kappa\, \rho\, c\, \left.\frac{\partial T}{\partial z}\right|_{\omega^+} \\ \text{diffu. heat inflow} & +\breve{\kappa}\, \breve{\rho}\, \breve{c}_p\, \left.\frac{\partial T}{\partial z}\right|_{\omega^-} \end{cases}
\end{aligned}
\tag{B2}
$$

where T_i the is initial temperature. Note that due to superheating within the melt layer the average temperature $\bar{T} = \frac{1}{\omega}\int_0^\omega T(z)\, dz$ is slightly above T_m. It is understtod that $\partial T/\partial z|_{\omega+}$ in referential z equates to $\partial T/\partial z|_{0+}$ in referential ξ of Eq. (11).

Within the melt , the heat balance should account for the shear heating $\tau\, V/2$ (considering one half layer of thickness ω), the inflow of new melt at temperature T_m, the extrusion of melt at an average temperature $\bar{T} > T_m$ and the diffusion toward the solid (radial diffusion is negligible, e.g. *Nielsen et al.*, 2008). As a consequence, considering a melt volume $S\,\omega$ where S is a given fault area, we may write the sum of all the heat sources, inflows and outflows and balance them with the increase of average temperature within the melt, such that:

$$
\begin{aligned}
&\left(\tfrac{\partial \bar{T}}{\partial t} \rho\, c_p\, \omega + \bar{T}\, \rho\, c_p\, \tfrac{\partial \omega}{\partial t}\right) S = \\
&\left(\breve{\rho}\ \breve{c}_p\, \breve{\nu}\, (T_m - T_i) - \breve{\rho}\, \breve{c}_p\, \dot{\omega}_c (\bar{T} - T_i) - \breve{\kappa}\, \breve{\rho}\, \breve{c}_p\, \left.\tfrac{\partial T}{\partial z}\right|_{\omega^-} + \tfrac{\tau\, V}{2}\right)\ S
\end{aligned}
\tag{B3}
$$

and get rid of the overall S factor to obtain the expression per unit fault surface:

$$
\begin{aligned}
&\tfrac{\partial \bar{T}}{\partial t} \rho\, c_p\, \omega + \bar{T}\, \rho\, c_p\, \tfrac{\partial \omega}{\partial t} = \\
&\breve{\rho}\, \breve{c}_p\ \left(\breve{\nu}\, (T_m - T_i) - \dot{\omega}_c (\bar{T} - T_i) - \breve{\kappa}\, \left.\tfrac{\partial T}{\partial z}\right|_{\omega^-}\right) + \tfrac{\tau\, V}{2}
\end{aligned}
\tag{B4}
$$

If the melt layer is thin ($\omega \ll 1$), the distributions of temperatures and heat sources within the melt layer are close to equilibrium (this does not exclude inhomogeneity and superheating above melting temperature). As a consequence, time variations within the melt are considered as small with respect to other terms, yeilding to assumption (I) of section 3 :

$$\breve{\kappa}\,\breve{\rho}\,\breve{c}_p \left|\frac{\partial T}{\partial z}\right|_{\omega^-} = \breve{\rho}\,\breve{c}_p\,\big(\breve{\nu}\,(T_m - T_i) - \dot{\omega}_c(\bar{T} - T_i)\big) + \frac{\tau\,V}{2\,\kappa\,\rho\,c_p} \tag{B5}$$

In order to obtain a solution of the shear heating problem, we neglect the heat difference of the two mass flows (melt inflow and extrusion), resulting in approximation (II) of section 3:

$$\breve{\rho}\,\breve{c}_p\,\big(\breve{\nu}\,(T_m - T_i) - \dot{\omega}_c(\bar{T} - T_i)\big) \ll \frac{\tau\,V}{2\,\kappa\,\rho\,c_p}\,. \tag{B6}$$

which finally results in the simple boundary condition:

$$\breve{\kappa}\,\breve{\rho}\,\breve{c}_p \left|\frac{\partial T}{\partial z}\right|_{\omega^-} = \frac{\tau\,V}{2\,\kappa\,\rho\,c_p} \tag{B7}$$

After some algebra, equation (B1) with boundary conditions (B7) and $T = T_m$ at the melt border, and the requirement of symmetry with respect to the center of the melt, result in the temperature and viscosity profiles of Eq (7) and Eq (8). Further details on the solution of the boundary problem can be found in *Nielsen et al.* [2008]. II.1bs

The validity of approximation (B6) is verified by computing both the complete expression (B5) and its approximation (B7) in the numerical examples shown in Fig. (11) and Fig. (12).

The friction melt problem is simulated under a normal stress of 10 MPa and under two successive velocity steps in slip (2 m/s and 1 m/s). Both the case where extrusion from a relatively small sample of 1 cm radius was computed (Fig. 11) and the case where no extrusion was allowed (Fig. 12). We represent the imposed slip rate and the computed shear stress for reference and superimepose the power density curves according to either Eq. (B5, dotted curve) and Eq. (B7 solid curve), in order to compare the full power to the approximate value used in the computation of melt temperature and viscosity profiles.

Upon comparison, we see that both curves almost always overalp and conclude that approximation (II) is reasonable. A slight misfit is observed only in the immediate vicinity of abrupt slip velocity changes. In particular, at the very initial onset of slip there is an underestimate of the power density "entering" the melt layer for a short time interval. This is because the melt layer in this phase is growing relatively faster than it is extruded, so neglecting the mass flows underestimates the entering heat flow, but the time duration of such misfit is extremely short and will not affect the resulting stress curve significantly. In addition, upon velocity negative stepping and arrest there is a slight overestimate during a short interval: in this phase the melt layer is thinning more rapidly than the rate of entering melt; as a result, neglecting mass flows underestimates some of the heat loss in these brief intervals if the velocity stepping is sufficiently abrupt. The consequence is that restrengthening in the very final slip phases may be slightly more enhanced than it appears using approximation (II). Overall Eq. (B7) shows minor misfits and offers a good approximate value for the solution of the shear heating problem.

Acknowledgments. S.N. and G.D.T. were supported by a European Research Council Starting Grant Project (acronym USEMS) and by a Progetti di Eccellenza Fondazione Cassa di Risparmio di Padova e Rovigo. We are grateful to Nick Beeler (and to an anonymous referee) for their constructive reviews and their help to improve the clarity of the manuscript.

References

Abercrombie, R., and J. Rice, Can observations of earthquake scaling constrain slip weakening?, *Geophys. J. Int.*, *162*, 406–424, 2005.

Beeler, N., Inferring earthquake source properties from laboratory observations and the scope of lab contributions to source physics, in *Earthquakes: Radiated energy and earthquake physics*, *Geophysical Monograph*, vol. 170, edited by R. Abercombie, A. McGarr, H. Kanamori, and G. D. Toro, American Geophysical Union, 2006.

Beeler, N., T. Tullis, and D. Goldsby, Constitutive relationships and physical basis of fault strength due to flash heating, *J. Geophys. Res.*, *113*(B1), B01,401, doi:10.1029/2007JB004988, 2008.

Bizzarri, A., and M. Cocco, A thermal pressurization model for the spontaneous dynamic rupture propagation on a three-dimensional fault: 1. methodological approach, *J. Geophys. Res.*, *111*, B05,303, 2006.

Brantut, N., A. Schubnel, J. Rouzaud, F. Brunet, and T. Shimamoto, High velocity frictional properties of a natural clay bearing fault gouge, *J. Geophys. Res.*, *113*, B10,401, doi:10.1029/2007JB005551, 2008.

Brodsky, E., and H. Kanamori, The elastohydrodynamic lubrication of faults, *J. Geophys. Res.*, *106*(B8), 16,357–16,374, 2001.

Brune, J., T. Henyey, and R. Roy, Heat flow, stress, and rate of slip along the san andreas fault, california, *J. Geophys. Res.*, *74*, 3821–3827., 1969.

Brune, J. N., S. Brown, and P. A. Johnson, Rupture mechanism and interface separation in foam ruber models of earthquakes: A possible solution to the heat flow solution and the paradox of large overthrusts, *Tectonophysics*, *218*, 59–67, 1993.

Cardwell, R., D. Chinn, G. Moore, and D. Turcotte, Frictional heating on a fault zone with finite thickness, *Geophys. J. Roy. Astr. Soc.*, *52*, 525–530, 1978.

Carslaw, H. S., and J. C. Jaeger, *Conduction of Heat in Solids*, Oxford University Press, USA, 1959.

Cocco, M., and E. Tinti, Scale dependence in the dynamics of earthquake propagation; evidence from seismological and geological observations, *Earth and Planetary Science Letters*, *273*, 123–131, 2008.

Crank, J., and P. Nicolson, A practical method for numerical evaluation of solutions of partial differential equations of the heat conduction type, *Proc. Camb. Phil. Soc.*, *43*, 50–67, 1947.

Del Gaudio, P., G. Di Toro, R. Han, T. Hirose, S. Nielsen, T. Shimamoto, and A. Cavallo, Frictional melting of peridotite and seismic slip, *J. Geophys. Res.*, *114*, B06,306, doi:10.1029/2008JB005990, 2009.

Di Toro, G., and G. Pennacchioni, Superheated friction-induced melts in zoned pseudotachylytes within the adamello tonalites (italian southern alps), *J. Struct. Geol.*, *26*, 1783–1801, 2004.

Di Toro, G., D. Goldsby, and T. Tullis, Friction falls towards zero in quartz rock as slip velocity approaches seismic rates, *Nature*, *427*, 436–439, 2004.

Di Toro, G., G. Pennacchioni, and G. Teza, Can Pseudotachylyte be used to infer earthquake source parameters? An example of limitations in the study if exhumed faults, *Tectonophysics*, *402*, 3–20, doi:10.1016/j.tecto.2004.10.014, 2005.

Di Toro, G., T. Hirose, S. Nielsen, G. Pennacchioni, and T. Shimamoto, Natural and experimental evidence of melt lubrication of faults during earthquakes, *Science*, *311*, 647–649, doi:10.1126/science.1121012, 2006a.

Di Toro, G., T. Hirose, S. Nielsen, and T. Shimamoto, Relating high-velocity rock-friction experiments to coseismic slip in the presence of melts, in *Radiated Energy and the Physics of Earthquake Faulting*, edited by R. Abercrombie, A. McGarr, H. Kanamori, and G. D. Toro, pp. 121–134, AGU, doi:10.1029/170GM13, 2006b.

Fialko, Y., and Y. Khazan, Fusion by earthquake fault friction: Stick or slip?, *J. Geophys. Res.*, *110*, B12407, doi:10.1029/2005JB003869, 2005.

Goldsby, D. L., and T. E. Tullis, Low frictional strength of quartz rocks at subseismic slip rates, *Geophys. Res. Lett.*, *29*, L01,240, doi:10.1029/2002GL01240, 2002.

Han, R., T. Shimamoto, T. Hirose, J.-H. Ree, and J. Ando, Ultralow friction of carbonate faults caused by thermal decomposition, *Science*, *316*, 878–881, doi:10.1126/science.1139763, 2007.

Heaton, T. H., Evidence for and implications of self-healing pulses of slip in earthquake rupture, *Phys. Earth Planet. Inter*, *64*, 1–20, corso, 1990.

Hirose, T., and T. Shimamoto, Growth of molten zone as a mechanicsm of slip weakening of simulated faults in gabbro during frictional melting, *J. Geophys. Res.*, *110*, B05202, doi:10.1029/2004JB003207, 2005.

Lachenbruch, A., Frictional heating, fluid pressure, and the resistance to fault motion, *J. Geophys. Res.*, *85*, 6097–6112, 1980.

Landau, H., Heat conduction in a melting solid, *Quart. Appl. Math.*, *8*, 81–94, 1950.

Lu, X., N. Lapusta, and A. J. Rosakis, Pulse-like and crack-like ruptures in experiments mimicking crustal earthquakes, *Proc. Natl. Acad. Sci. USA*, *104*, 18,931–18,936, 2007.

Melosh, J., Dynamic weakening of faults by acoustic fluidization, *Nature*, *397*, 601–606, 1996.

Nielsen, S., and R. Madariaga, On the self-healing fracture mode, *Bull. Seismol. Soc. Am.*, *93*(6), 2375–2388, doi:10.1785/0120020090, 2003.

Nielsen, S., G. Di Toro, T. Hirose, and T. Shimamoto, Frictional melt and seismic slip, *J. Geophys. Res.*, *113*, B01,308, doi:10.1029/2007JB005122, 2008.

Nielsen, S., G. Di Toro, and W. A. Griffith, Friction and roughness of a melting rock surface, *Geophys. J. Int. (under review)*, 2009.

Nielsen, S. B., and J. M. Carlson, Rupture pulse characterization: Self-healing, self-similar, expanding solutions in a continuum model of fault dynamics, *Bull. Seismol. Soc. Am.*, *90*(6), 1480–1497, doi:10.1785/0120000021, 2000.

Niemeijer, A., et al., A new state-of-the-art tool to investigate rock friction under extreme slip velocities and accelerations: Shiva, in *Eos, Trans., AGU Fall Meeting Suppl.*, vol. **90**(52), American Geophysical Union, abs. T23C-1950, 2009.

Peachman, D. W., and H. H. Rachford, The numerical solution of parabolic and elliptic differential equations, *J. Soc. Industrial Appl. Math.*, *3*, 1–28, 1955.

Rempel, A., and S. Weaver, A model for flash weakening by asperity melting during high-speed earthquake slip, *Journal of Geophysical Research*, *113*(B11), B11,308, doi:10.1029/2008JB005649, 2008.

Rice, J. R., Heating and weakening of faults during earthquake slip, *J. Geophys. Res.*, *111*, B05311, doi:10.1029/2005JB004006, 2006.

Shand, The pseudotachylyte of parijs (orange free state) and its relation to trapp-shotten gneiss and flinty crush rock, *Quart. J. Geol. Soc. London,*, *72*, 198–221, 1916.

Shimamoto, T., and A. Tsutsumi, A new rotary-shear high-velocity frictional testing machine: Its basic design and scope of research, *Struct. Geol.*, *39*, 65–78, (in Japanese with English abstract), 1994.

Sibson, R., Generation of pseudotachylyte by ancient seismic faulting, *Geophys. J. R. Astron. Soc.*, *43*, 775–794, 1975.

Sirono, S., K. Satomi, and S. Watanabe, Numerical simulations of frictional melting: Small dependence of shear stress drop on viscosity parameters, *J. Geophys. Res.*, *111*, B06309, doi:10.1029/2005JB003858, 2006.

Snoke, A., J. Tullis, and V. Todd, *Fault Related Rocks. A photographic Atlas*, Princeton, 1998.

Sone, H., and T. Shimamoto, Frictional resistance of faults during accelerating and decelerating earthquake slip, *Nature Geoscience*, doi:10.1038/NGEO637, 2009.

Spray, J., Artificial generation of pseudotachylyte using friction welding apparatus: simulation of melting on a fault plane, *J. Struct. Geol.*, *9*, 49–60, 1987.

Spray, J., A physical basis for the frictional melting of some rock forming minerals, *Tectonophysics*, *204*, 205–221, 1992.

Spray, J. G., Evidence for melt lubrication during large earthquakes, *Geophys. Res. Lett.*, *32*, L07,301, doi:10.1029/2004GL022293, 2005.

Spudich, P., Use of fault striations and dislocation models to infer tectonic shear stress during the 1995 Hyogo-ken Nanbu (Kobe), Japan, earthquake, *Bull. Seismol. Soc. Am.*, *88*, 413–427, 1998.

Swanson, M., Fault structure, wear mechanisms and rupture processes in pseudotachylyte generation, *Tectonophysics*, *204*, 223–242, 1992.

Tinti, E., P. Spudich, and M. Cocco, Earthquake fracture energy inferred from kinematic rupture models on extended faults, *J. Geophys. Res.*, *110*, B12,303, doi:10.1029/2005JB003644, 2005.

Tinti, E., M. Cocco, E. Fukuyama, and A. Piatanesi, Dependence of slip weakening distance (d (sub c)) on final slip during dynamic rupture of earthquakes, *Geophysical Journal International, vol. 177, no. 3, pp.1205-1220, Jun 2009*, *177*, 1205–1220, 2009.

Tsutsumi, A., and T. Shimamoto, High-velocity frictional properties of gabbro, *Geophys. Res. Lett.*, *24*, pp.699–702, 1997.

Ueda, T., M. Obata, G. Di Toro, K. Kanagawa, and K. Ozawa, Mantle earthquakes frozen in mylonitized ultramafic pseudotachylytes of spinel-lherzolite facies, *Geology*, *36(8)*, 607–610, 2008.

Whittington, A. G., A. M. Hofmeister, and P. I. Nabelek, Temperature-dependent thermal diffusivity of the Earth's crust and implications for magmatism, *Nature*, *458*, 319–321, doi:10.1038/nature07818, 2009.

Zheng, G., and J. Rice, Conditions under which velocity weakening friction allows a self-healing versus a cracklike mode of rupture, *Bull. Seismol. Soc. Am.*, *88*(6), 1466–1483, 1998.

	Rock	Gabbro	Peridotite	Tonalite
ρ	kg m^{-3}	3000	3230	2800
c_p	J kg^{-1} ^{o} C^{-1}	950	850	755
κ	m^2 s^{-1}	0.48 10^{-6}	1.27 10^{-6}	2.8 10^{-6}
L	J kg^{-1}	350 10^3	560 10^3	332 10^3
T_m	^{o}C	1400	1600	1200
ΔT	^{o}C	100	100	500
σ_c	MPa	150	150	150
η_c	Pa s	6.5 10^3	3.0 10^3	20 10^3
W	m s^{-1}	0.2	0.08	0.2
T_c	^{o}C	23.8	0.68	16.9
H	m^{-1}	0.22	0.03	0.1

Table 1. Parameters used in models for various rocks. The very low value of indentation hardness assumes that minerals on the sliding surface are close to their melting temperature.

exp. #	σ_n (MPa)	V (m/s)
HVR687	15.5	1.14
HVR688	5.12	1.14
HVR689	1.2	1.14
HVR690	2.5	1.14
HVR724	1.0	1.8
HVR723	0.9	1.36
HVR725	2.0	1.36
HVR726	1.5	1.82
HVR727	1.0	1.82
HVR737	2.0	1.81
HVR765	1.5	2.18
HVR729	1.0	1.83

Table 2. Normal stress and slip velocity imposed during the HVRF experiments performed on gabbro [*Nielsen et al.*, 2008] and used in Fig. (7, crosses).

Figure 1. Comparison of friction evolution from experiment HVR373 performed o n tonalite (thin black curves) with numerical model (grey curves). Experimental conditions were $\sigma_n = 15\,\mathrm{MPa}$, $V = 1.26\,\mathrm{m/s}$ *Di Toro et al.* [2006a]. The parameters used for modelling Tonalite are specified in Table 1.

Data from (Sibson, 1975)			
Separation mm	Thickness mm	Thick./Sep.	Shear stress MPa
7.0	0.5	0.071	339
3.4	0.2	0.059	279
28.0	1.3	0.045	212
18.0	0.5	0.028	132
67.0	1.5	0.022	106
88.0	1.8	0.020	94
82.0	1.5	0.018	87
71.0	1.3	0.018	84
58.0	1.0	0.017	82
117.0	2.0	0.017	81
68.0	0.8	0.011	52
243.0	2.3	0.009	44
1290.0	7.5	0.006	28
910.0	3.3	0.004	17

Table 3. Field data from a thrust fault zone in Outer Hebrides, Scotland. The set shows data from [*Sibson*, 1975] used for figure 9 in combination with and original data from a 2005 survey (shown in Table 4). For the estimate of shear stress as of Eq. (21) we use $E = 1.76$ MJ/kg and $\rho = 2800$ kg m^{-3} [*Sibson*, 1975]. Separation (and Sep. in third column) refer to the distance measured between separation markers on the exposed fault section (see text for details).

Figure 2. Comparison of friction evolution from experiment HVR620 performed on peridotite (thin black curves) with numerical model (grey curves). Experimental conditions were $\sigma_n = 13\,\mathrm{MPa}$, $V = 1.14\,\mathrm{m/s}$ [*Del Gaudio et al.*, 2009]. The parameters used for modelling peridotite are specified in Table 1.

(a)

Figure 3. (a) Comparison of friction evolution from experiment HVR621 performed on peridotite (thin black curves) with numerical model (grey curves). (b) Slip velocity stepping imposed. Experimental conditions were $\sigma_n = 10.4\,\mathrm{MPa}$, variable V as shown [*Del Gaudio et al.*, 2009]. The parameters used for modelling peridotite are specified in Table 1.

Data from Hirose (unpublished)			
Separation mm	Thickness mm	Thick./Sep.	Shear stress MPa
22.0	0.3	0.014	65
24.0	1.1	0.046	218
12.0	0.7	0.054	257
55.0	1.4	0.025	117
31.0	0.4	0.013	61
26.0	0.2	0.007	33
80.0	1.4	0.018	83
25.0	0.5	0.018	85
18.0	0.8	0.044	211
65.0	0.8	0.012	58
75.0	1.4	0.019	89
43.0	0.4	0.009	44
65.0	0.3	0.005	22
57.0	0.6	0.011	50
420.0	3.1	0.007	35
630.0	2.8	0.004	21
480.0	1.9	0.004	19
78.0	1.6	0.021	99
49.0	0.4	0.009	42
94.0	1.3	0.014	66
82.0	0.7	0.008	39
150.0	1.8	0.012	57
310.0	1.4	0.005	22
59.0	0.6	0.011	51
275.0	1.3	0.005	22
685.0	2.8	0.004	19
35.0	0.4	0.011	54
43.0	0.5	0.012	59
41.0	0.6	0.013	64
76.0	0.7	0.009	45
120.0	0.7	0.006	28
46.0	0.3	0.007	31
11.0	0.5	0.043	203
1670.0	1.8	0.001	5

Table 4. Contination of Table 3

Figure 4. Comparison of friction evolution from experiment HVR687 performed on gabbro (thin black curves) with numerical model (grey curves). Note that at around 9.5 s the sample broke causing the erratic rise in frictional data. Experimental conditions were $\sigma_n = 15.5\,\mathrm{MPa}$, $V = 1.14\,\mathrm{m/s}$ [*Nielsen et al.*, 2008]. The parameters used for modelling gabbro are specified in Table 1.

Figure 5. (a) Comparison of friction evolution from experiment HVR727 performed on gabbro (thin black curves) with numerical model (grey curves). (b) Slip velocity stepping imposed. Experimental conditions were $\sigma_n = 1.0\,\mathrm{MPa}$, variable V as shown [*Nielsen et al.*, 2008]. The parameters used for modelling gabbro are specified in Table 1.

Figure 6. Comparison of friction evolution from experiment HVR688 performed on gabbro (thin black curves) with numerical model (grey curves). Experimental conditions were $\sigma_n = 5.12\,\mathrm{MPa}$, $V = 1.14\,\mathrm{m/s}$ [*Nielsen et al.*, 2008]. The parameters used for modelling gabbro are specified in Table 1. In this example we also show the (a) experimental and numerical shortening, in black and grey curves respectively, (b) the thickness and (c) maximum melt temperature (about 100^oC above melting temperature T_m).

Figure 7. General trends of (a) weakening time t_{th}, (b) thermal weakening distance D_{th} , (c) steady state shear stress τ_{ss}, for suitable combinations of normal stress σ_n and slip velocity V. (d-e) show that breakdown energy W_b is virtually independent of either σ_n and slip velocity V; the shaded area indicates the range of breakdown energy estimated from seismological data in the literature [*Abercrombie and Rice*, 2005; *Tinti et al.*, 2005; *Cocco and Tinti*, 2008; *Tinti et al.*, 2009]. The values represented as disks were obtained using Gabbro parameters (see Table 1) and performing simulations of transient evolution of friction, under different combinations of slip velocity ($V = 1$m/s in light gray, $V = 3$m/s in gray, $V = 9$m/s in black) and variable normal stress ($1 < \sigma_n < 64$ MPa). Crosses are estimates form twelve HVRF experiments preformed on gabbro (see Table 2). In (c), the effect of α (Eq. 13) on the normal stress causes a departure from the general trend in both model and data, but only for those tests performed at lower slip rates (V=1 m/s); indeed α becomes negligible at higher slip rates [*Nielsen et al.*, 2009]. For reference, dotted lines with log-log slopes in -1 (a,b) and +1/4 (c) are represented. See text for further details.

Figure 8. Dependence of shear stress on melt extrusion radius R. Each curve corresponds to a given extrusion radius as indicated, in centimeters, for R=0.25, 1, 4 and ∞ (the last case is equivalent to no extrusion). The imposed slip rate stepping is indicated as a dashed curve. The normal stress is $\sigma_n = 10$ MPa. We note that for R $\gtrsim 4\,$cm the solution is almost identical to the case with no extrusion ($\mathrm{R} = \infty$). Finally, the convergence time to steady state increases with R until no steady state can be reached for $\mathrm{R} = \infty$.

Figure 9. Comparison of shear stress estimate from field data on exhumed seismic faults and results from the model of melt and heat diffusion. Outlayers are data points concerning very thin pseudotachylite and short separation measures, so that large errors of a factor of 2 or more are expected. See text for further details.

Figure 10. Friction under a continuously varying slip rate function expected in a dynamic earthquake rupture. Slip rate corresponds to the dynamic solution for a self-healing pulse proposed by *Nielsen and Madariaga* [2003], with a total rise time of 5s. The [*Nielsen and Madariaga*, 2003] solution was smoothed in order to remove the initial singularity (using a Gaussian moving average of with standard deviation of 0.2 s) resulting in an initial ramp of about 0.6 s. Friction was computed under either (a) $\sigma_n = 10\,\mathrm{MPa}$ and (b) $\sigma_n = 64\,\mathrm{MPa}$. Extrusion radii of either $\mathrm{R} = 1\,\mathrm{cm}$ (dotted curves) or $\mathrm{R} = \infty$ (solid curves) were used in the model. In all cases the weakening is very fast and there is considerable hardening as the slip rate drops in the later part of the slip function.

Figure 11. Test of approximation (II) for a model with an extrusion radius of 1 cm. (c): Comparison between power density value used in approximation II (solid curve) and the actual power density value (dotted curve). For reference, (a) shows the imposed velocity steps and (b) shows the resulting stress curve.

Figure 12. Test of approximation (II) for a model with no extrusion. (c): Comparison between power density value used in approximation II (solid curve) and the actual power density value (dotted curve). For reference, (a) shows the imposed velocity steps and (b) shows the resulting stress curve.

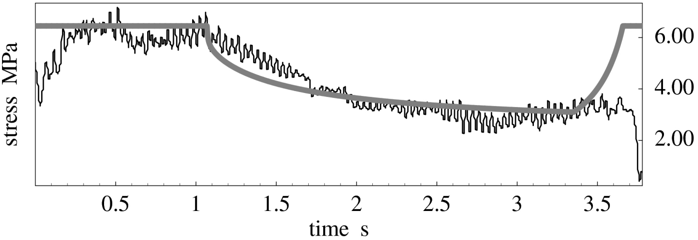

Figure 1: Nielsen et al.

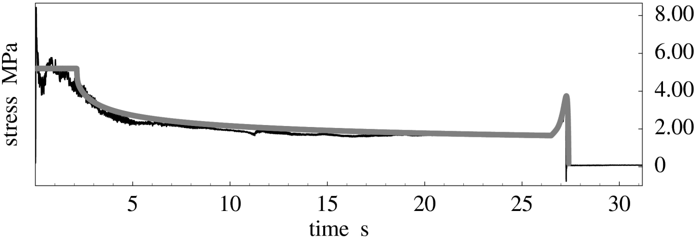

Figure 2: Nielsen et al.

(a)

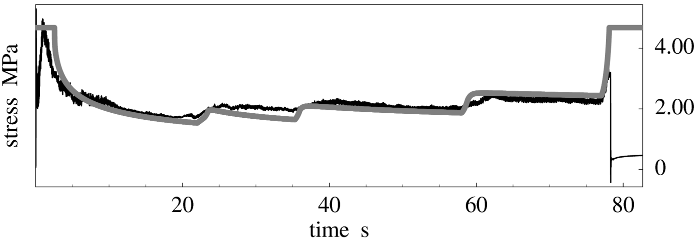

(b)

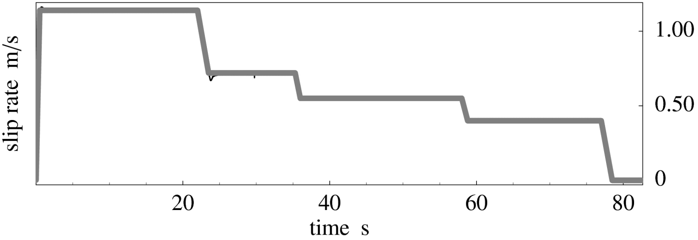

Figure 3: Nielsen et al.

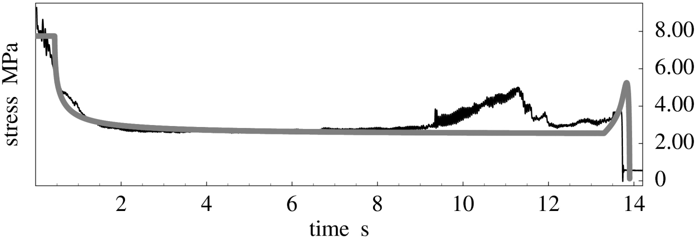

Figure 4: Nielsen et al.

(a)

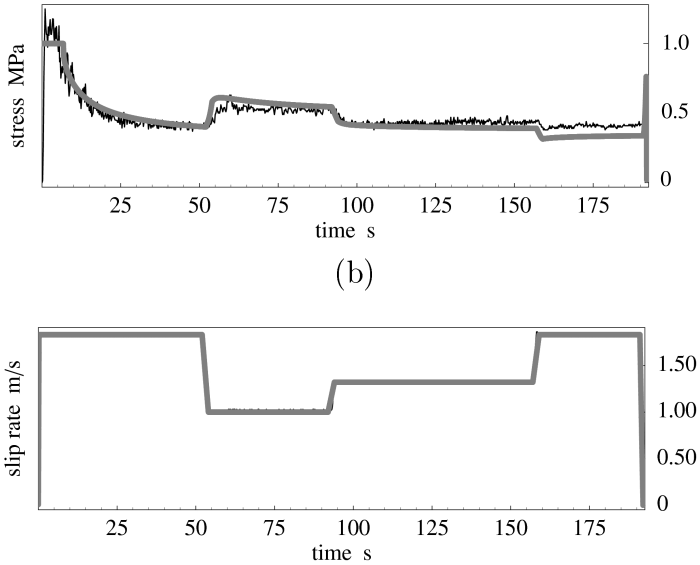

(b)

Figure 5: Nielsen et al.

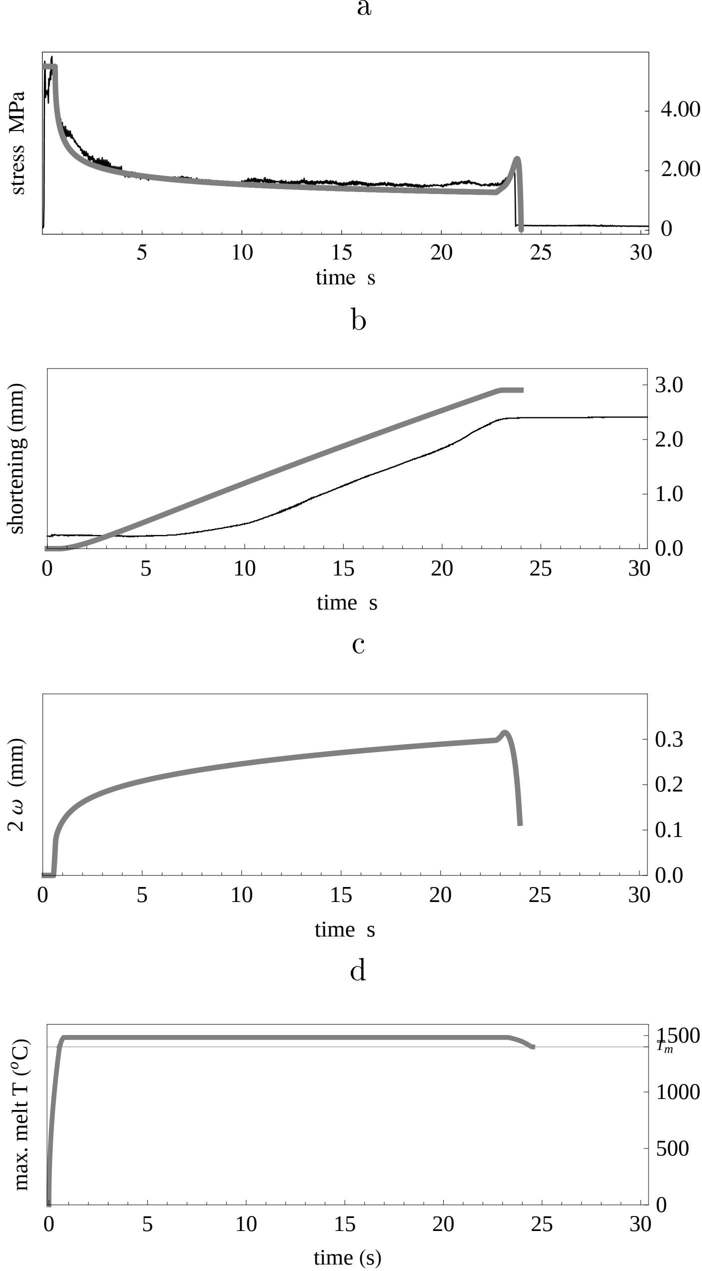

Figure 6: Nielsen et al.

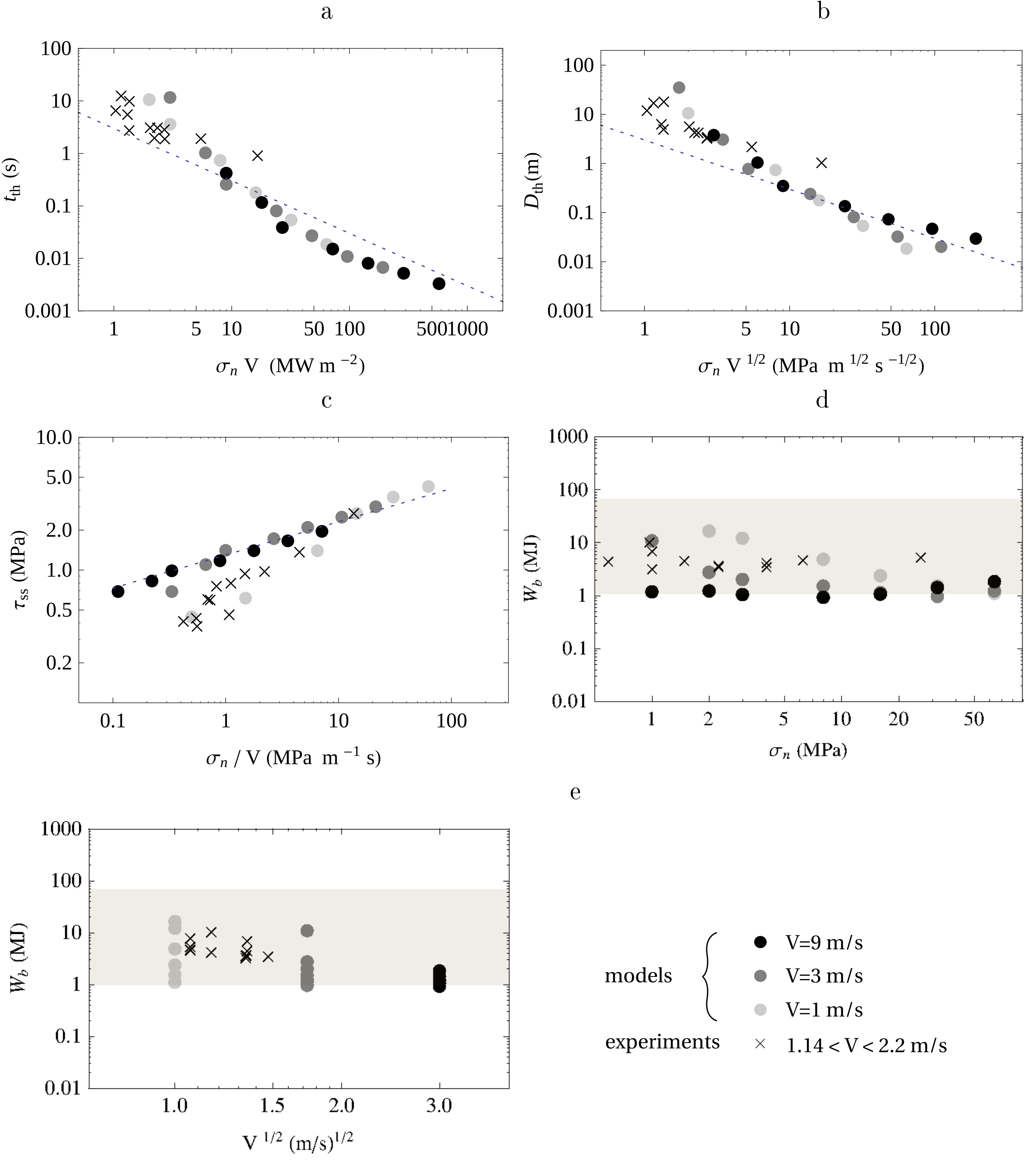

Figure 7: Nielsen et al.

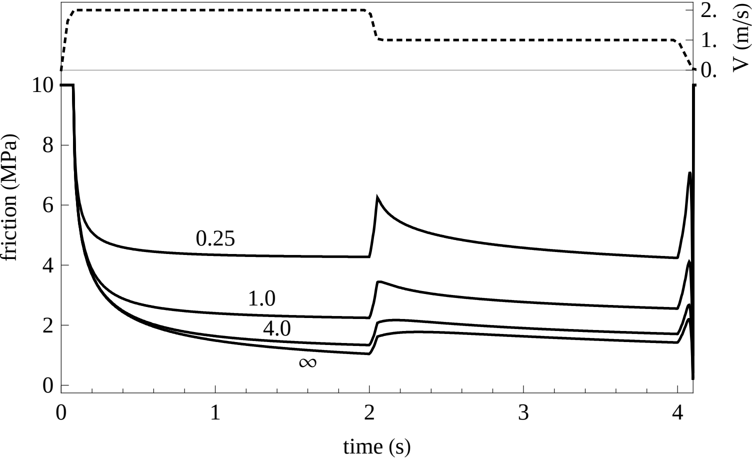

Figure 8: Nielsen et al.

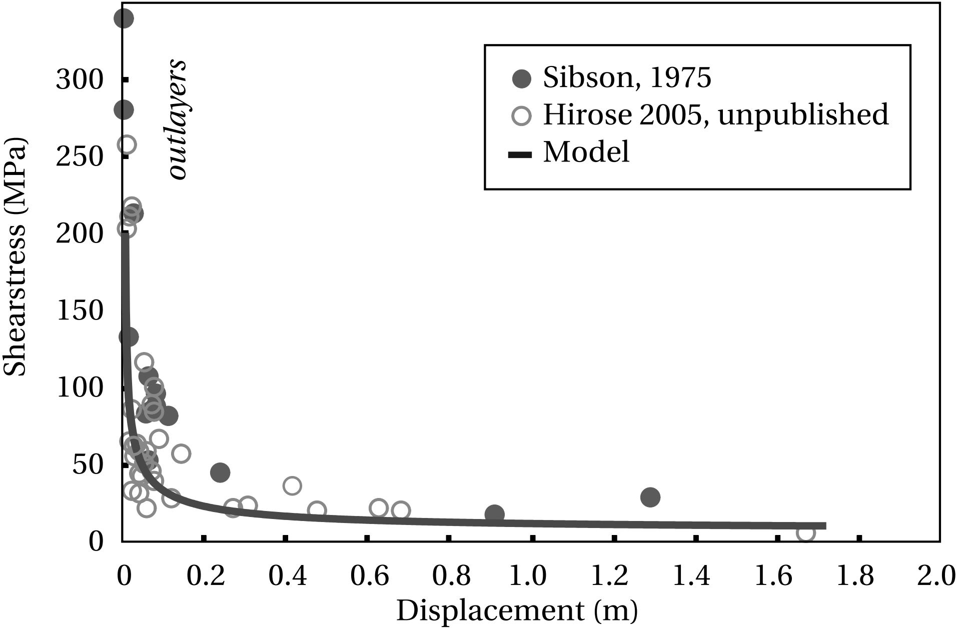

Figure 9: Nielsen et al.

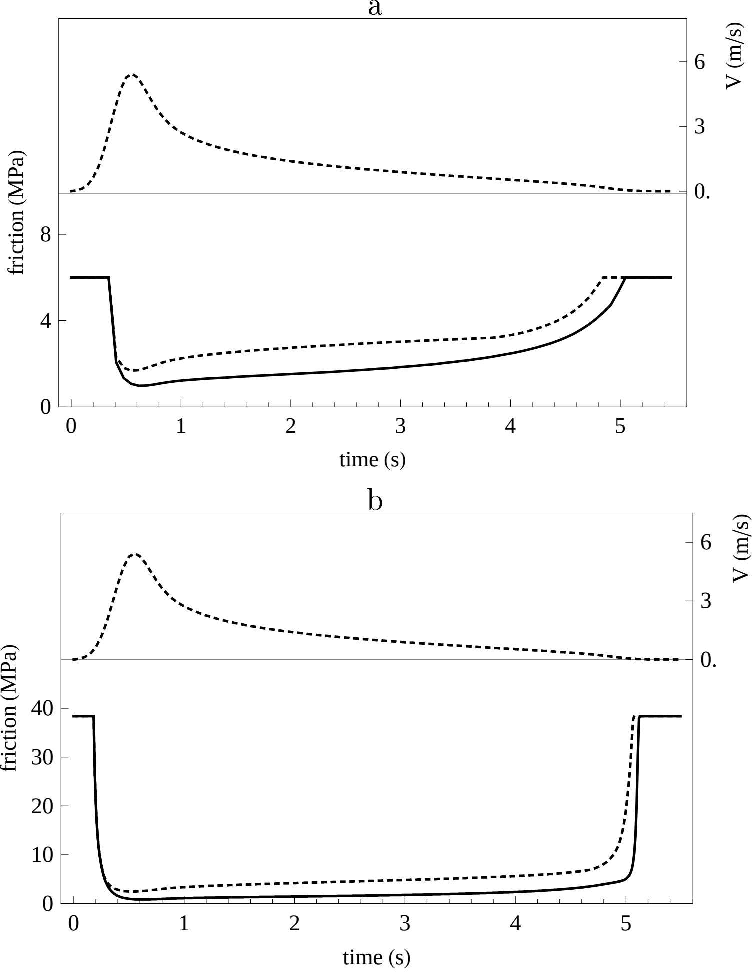

Figure 10: Nielsen et al.

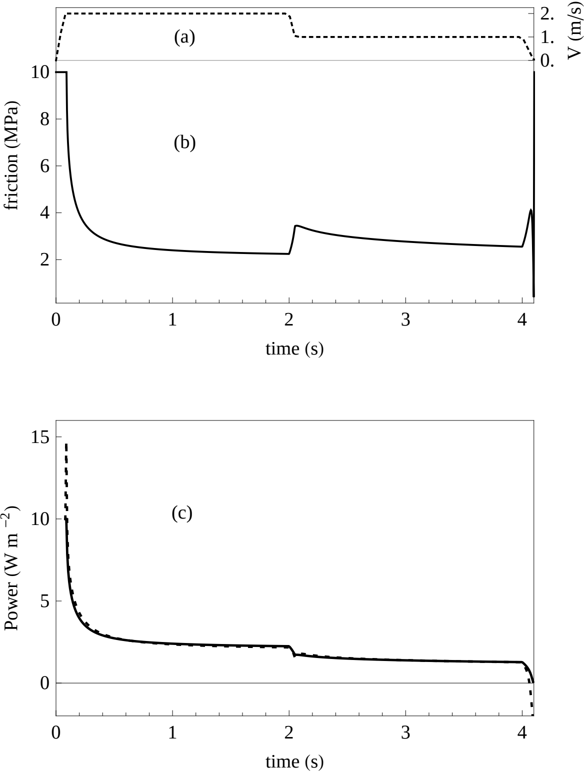

Figure 11: Nielsen et al.

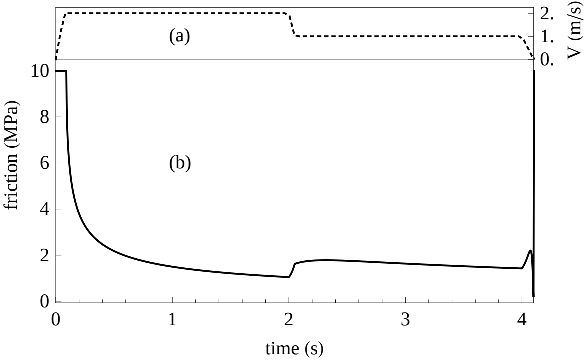

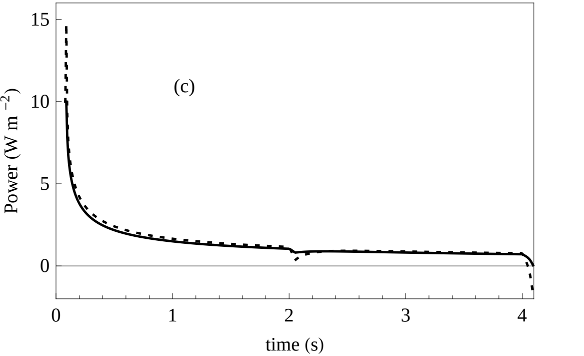

Figure 12: Nielsen et al.